Comprehensive Genome Based Analysis of *Vibrio parahaemolyticus* for Identifying Novel Drug and Vaccine Molecules: Subtractive Proteomics and Vaccinomics Approach

Mahmudul Hasan[1], Kazi Faizul Azim[2], Abdus Shukur Imran[1], Ishtiak Malique Chowdhury[3], Shah Rucksana Akhter Urme[4], Md Sorwer Alam Parvez[5], Md Bashir Uddin[6*], Syed Sayeem Uddin Ahmed[7*]

[1]Department of Pharmaceuticals and Industrial Biotechnology
Sylhet Agricultural University, Sylhet-3100, Bangladesh

[2]Department of Microbial Biotechnology
Sylhet Agricultural University, Sylhet-3100, Bangladesh

[3]Department of Molecular Biology and Genetic Engineering
Sylhet Agricultural University, Sylhet-3100, Bangladesh

[4]Department of Biochemistry and Chemistry
Sylhet Agricultural University, Sylhet-3100, Bangladesh

[5]Department of Genetic Engineering and Biotechnology
Shahjalal University of Science and Technology, Sylhet-3114, Bangladesh

[6]Department of Medicine, Sylhet Agricultural University, Sylhet-3100, Bangladesh

[7]Department of Epidemiology and Public Health, Sylhet Agricultural University, Sylhet-3100, Bangladesh

***Correspondence**

bashir.vetmed@sau.ac.bd [MB Uddin]

ahmedssu.eph@sau.ac.bd [SSU Ahmed]

Identifying Novel Drug and Vaccine Molecules of *Vibrio parahaemolyticus* by Subtractive Proteomics and Vaccinomics Approach

Abstract

Multidrug-resistant *Vibrio parahaemolyticus* has become a significant threat to human health as well as aquaculture, prioritizing the development of effective drug and vaccine candidates. Hence, the study was designed to identify novel therapeutics using a comprehensive genome-based analysis of *V. parahaemolyticus.* From *V. parahaemolyticus* proteome, a total of 4822 proteins were investigated in order to find out effective drug and vaccine targets. A range of diverse subtractive proteomics approaches – namely, identification of human non-homologous and pathogen-specific essential proteins, druggability and 'anti-target' analysis, prediction of subcellular localization, human microbiome non-homology screening, analysis of virulence factors, protein-protein interactions studies. Among 16 novel cytoplasmic proteins, 'VIBPA Type II secretion system protein L' and 'VIBPA Putative fimbrial protein Z' were allowed to molecular docking with 350 human metabolites, which revealed that Eliglustat, Simvastatin and Hydroxocobalamin were the top drug molecules considering free binding energy. On the contrary, 'Sensor histidine protein kinase UhpB' and 'Flagellar hook-associated protein of 25 novel membrane proteins were subjected to T and B cell epitope prediction, antigenicity testing, transmembrane topology screening, allergenicity and toxicity assessment, population coverage analysis and molecular docking were adopted to generate the most immunogenic epitopes. Three subunit vaccines were constructed by the combination of highly antigenic epitopes along with suitable adjuvant, PADRE sequence and linkers. The designed vaccine constructs (V1, V2, V3) were analyzed by their physiochemical properties and molecular docking with MHC molecules that suggested the superiority of construct V1. Besides, the binding affinity of human TLR1/2 heterodimer and construct V1 was also biologically significant. The vaccine-receptor complex exhibited deformability at a minimum level that also strengthened our prediction. The

optimized codons of the designed construct was cloned into pET28a(+) vector of *E. coli* strain K12. However, the predicted drug molecules and vaccine constructs could be further studied to combat *V. parahaemolyticus* associated infections.

Keywords: *Vibrio parahaemolyticus*, Subtractive Proteomics, Vaccinomics, Drug Targets, Gastroenteritis, Molecular Docking

Introduction

Vibrio parahaemolyticus, a highly reported pathogenic bacteria of aquatic environment, belongs to vibrionaceae family has emerged as the leading cause of seafood-associated gastroenteritis and a significant hazard for global aquaculture (Tang et al., 2014, Ghenem et al., 2017, Chen et al., 2017, Letchumanan et al., 2014). The overgrowing population, with increased purchasing power worldwide, has enhanced the demand for and export potential of seafood, resulting in the steady expansion of the aquaculture industry (Rico et al., 2012). However, the sector has continuously been challenged by aquatic animal health problems, which are a significant constraint to the development of this sector (Bondad-Reantaso et al., 2005). Besides, Antimicrobial resistance

(MDR) has been recognized as an essential global threat issue to food safety (Food and Agriculture Organization, 2016). The continuous and inappropriate use of antibiotics in the aquaculture industry favors the development of a variety of resistant isolates and the dissemination of resistance genes within the bacterial population (Tendencia and de laPena, 2001). *V. parahaemolyticus* has been reported to show multidrug resistance during aquaculture production (Vaseeharan et al., 2005; Han et al., 2007, Yang et al., 2017), which raised the concern about public health and economic threat of this bacterium (Lesley et al., 2011; Noorlis et al., 2011; Osunla et al., 2017).

Though *V. parahaemolyticus* was first isolated in 1952, reports demonstrated the recent outbreaks of *V. parahaemolyticus* are more severe (Jung, 2018; Liu et al., 2015; Jang et al., 2013). On the recent outbreak in the city of Osaka (Japan), acute gastroenteritis was reported in 272 individuals, 20 of whom died (Daniels et al., 2000). To date, *V. parahaemolyticus* has been responsible for 20–30% of food poisoning cases in Japan and sea foodborne diseases in many Asian countries (Alam et al., 2002). A total 802 outbreaks of food-borne diseases have been reported in 13 of the coastal provinces of eastern China, causing more than 17,000 individuals to become ill (Wang et al., 2011a; Wu et al., 2014), where *V. parahaemolyticus* attributed the most significant number (40.1%) of these cases (Liu et al., 2006, Nair et al., 2007, Chao et al., 2011). The leading cause of human gastroenteritis associated with seafood consumption in the United States is *V. parahaemolyticus* (Kaysner and De Paola, 2001; Newton et al., 2012). Centers for Disease Control and Prevention (CDC) declared it as a significant foodborne bacterium compared to other *Vibrio* species, which was responsible for approximately 34,664 foodborne cases annually in the USA (Scallan et al., 2011; Huang et al., 2016).

The food poisoning caused by *V. parahaemolyticus* usually occurs in summer and is predominantly associated with different kinds of seafood, including crab, shrimp, shellfish, lobster, fish and oysters (Cruz et al, 2015; Letchumanan et al., 2015). *V. parahaemolyticus* is usually found in a free-swimming state, with its motility conferred by a single polar flagellum affixed to inert and animate surfaces including zooplankton, fish, shellfish or any suspended matter underwater (Gode-Potratzetal, 2011). Among the whole range of seafood, shellfish is regarded as a high-risk food because it is infested with large populations of bacteria, including *V. parahaemolyticus* (Peng et al., 2010; China Statistical Yearbook, 2012). Illness is inevitable, once consumers eat undercooked

contaminated seafood (Rahimi et al., 2010). The symptoms of the disease include diarrhea, vomiting, abdominal pain, nausea and low-grade fever (Ham and Orth, 2012). In most cases, the disease is self-resolving. However, *V. parahaemolyticus* may cause a more debilitating and dysenteric form of gastroenteritis (Levin, 2006). Uncommonly, in immunocompromised patients, it may progress into a life-threatening fulminant necrotizing fasciitis characterized by rapid necrosis of subcutaneous tissue (Ahmad et al., 2013). In rare cases, *V. parahaemolyticus* causes septicemia, which is also associated with a high mortality rate (Zhang and Orth, 2013). Also, *V. parahaemolyticus* is one of the major pathogens of cultured mud crabs and cause acute hepatopancreatic necrosis disease (AHPND) in shrimp (Xiao et al., 2017). Usually, 99% of clinical *V. parahaemolyticus* isolates are known to be pathogenic, whereas the majority of the environmental isolates are non-pathogenic (Yu et al., 2013; Sudha et al., 2014). Nonetheless, around 0–6% of the environmental isolates are identified as pathogenic carrying virulence genes (Letchumanan et al., 2014). During infection, *V. parahaemolyticus* uses the adhesion factors to bind to the fibronectin and phosphatidic acid on the host cell, thus releasing different effectors and toxins into the cytoplasm, causing cytotoxicity and serious diseases (Gode-Potratz et al., 2011).

Many antibiotics are no longer effective in hospitals to treat *V. parahaemolyticus* infections (Tan et al., 2016, Jun et al., 2014, Lin et al., 2017). First-generation antibiotics, including ampicillin are extensively used in aquaculture resulting in reduced susceptibility and low efficacy of ampicillin for *Vibrio* sp. treatment (Sudha et al., 2014, Han et al., 2007). Literature also reported higher resistance to third-generation antibiotics such as cephalosporin, cefotaxime, carbapenems and ceftazidime by *V. parahaemolyticus* isolates (Lee et al., 2018; Jun et al., 2012; Letchumanan et al., 2015) which enhanced the necessity of searching safe and more effective drugs for combating infections caused by *V. parahaemolyticus* in the future. However, the development of new antibiotics is difficult and time-consuming. Recent progress in the field of computational biology and bioinformatics has generated various in silico analysis and drug designing approaches. Thus eliminating the time and cost involved in the early trial phase before going into the drug development phase (Barh et al., 2011). Subtractive genomics is one such in silico strategy that helps to facilitate the selection, processing, and development of strain-specific drugs against various pathogens (Azim et al., 2019). It can be utilized to identify drug targets based on the determination of essential and nonhomologous proteins within the pathogenic organism (Barh and Kumar, 2009; Hosen et al., 2014). Various novel drug targets have already been successfully

identified for *S. typhi meningitides*sero group B (Perumalet al., 2007; Barh and Kumar, 2009) using the mentioned approach.

Moreover, *in silico* docking studies between the identified drug targets and existing drugs with slight modification may lead to the discovery of novel drugs for the treatment of infections (Pagadala et al., 2017; Wong, 2015; Ferreira et al., 2015; Yuriev et al., 2013). As a result, a wide range of drug targets and lead compounds can be identified before laboratory experimentation, to save time and money. The study was designed to employ a comprehensive genome-based analysis of *Vibrio parahaemolyticus* for identifying novel therapeutic targets as well as suitable drug and vaccine molecules through subtractive proteomics and vaccinomics approaches.

Results

Various bioinformatics tools and databases were used to analyze the entire proteome of *V. parahemolyticus* through subtractive genomics and vaccinomics approach. The step by step results (or workflow in Fig. 1 and Fig. 2) from the complete computational analysis was presented in Table 1.

Retrieval of complete proteome and identification of essential proteins

The whole proteome of *V. parahemolyticus* strain O3:K6 was extracted from NCBI database (Supplementary file 1) containing 4822 proteins (Set 0). Paralogous protein sequences of the pathogen. A total of 93 paralogous sequence above >60% similarity were identified through the CD-hit server and removed, leaving 4729 non-paralogous protein sequences in Set 1 (Supplementary file 2). Among these proteins, proteins with >100 residues (4123 proteins) (Set 2) were only considered (Supplementary file 3) for further analysis. Again, proteins showing significant similarity with human RefSeq proteins (1143 proteins) were excluded from the list designated as Set 3 (Supplementary file 4). Analysis of remaining proteins through the DEG server revealed only proteins that are essential (Set 4) for the survival of the pathogen (Supplementary file 5).

Analysis of Metabolic pathways

The KEGG server contains 131 metabolic pathways for *V. parahaemolyticus* (Supplementary file 6) and 325 pathways for humans (Supplementary file 7). Through manual comparison, 40 metabolic pathways were found to be pathogen-specific and are provided in Supplementary file 8. Proteins involved in these unique pathways can be selected as drug targets. Non-homologous essential proteins subjected to BLASTp in the KAAS server at KEGG revealed that 96 proteins among 1107 assigned both KO (KEGG Orthology) and metabolic pathways that further deputed as Set 5 (Supplementary file 9).

Druggability analysis and identification of novel drug targets

Only 56 proteins showed similarity with the available drug targets, while the remaining 41 showed no hit. These 41 proteins (Set 6) were considered as novel drug targets which include both cytoplasmic and membrane proteins (Supplementary file 10). Besides, the results of druggable proteins are provided in supplementary table 1. Furthermore, the other 41 proteins were considered as novel therapeutic targets and subjected to human ‘anti-targets’ analysis.

‘Anti-target’ analysis and prediction of subcellular localization

A total of 210 ‘anti-targets’ reported in the literature were fetched from NCBI (Supplementary file 11). All novel drug target proteins were successfully screened through BLASTp analysis, and no evidence of similarity was seen. Hence, all these novel drug target proteins were listed for human microbiome analysis considering non-homologous to host ‘anti-targets’ (Supplementary file 10). Moreover, The results of subcellular localization analysis by four servers are provided in Supplementary file 11. The result revealed that among 41 specific proteins involved in pathogen-specific pathways, 16 were cytoplasmic proteins assigned as Set 8 (Supplementary file 12, Table 2), while the remaining 25 sequences were membrane proteins.

Human microbiome non-homology analysis

Cytoplasmic proteins showing <45% similarity with reported human microbiome proteins were selected for protein-protein interaction analysis, whereas membrane proteins were selected for further vaccine candidacy. However, microbiome analysis revealed that a total of 9 proteins (Set 9) of the pathogen showed <45% similarity with human microflora (Supplementary Table 2, Supplementary file 13).

Analysis of virulence factors (VF's) and protein-protein interactions studies (PPIs)

From 9 cytoplasmic novel proteins, five uncharacterized proteins were removed and the remaining four proteins were considered for VFDV analysis. The VFDB result showed that two proteins (Set 10) i.e., VIBPA Type II secretion system protein L (Q87TC9) and VIBPA Putative fimbrial protein Z (Q87I65) were associated with virulence of *V. parahaemolyticus* (Table 3). These proteins were subjected to protein-protein interaction study. STRING v10.5 revealed that Type II secretion system protein L confers interactions with nine proteins (Fig. 3A), while putative fimbrial protein Z exhibits interactions with three other proteins (Fig. 3B). These proteins are mainly responsible for protein transport, involved in biofilm formation and bacterial secretion system, or act as regulatory proteins (e.g., transcription regulator, signal transduction response regulator).

Screening of drug molecules against novel cytoplasmic proteins

A total of 335 unique metabolites were retrieved from Human Metabolites Database for docking analysis against predicted therapeutic drug targets (novel cytoplasmic proteins). Docking scores were analyzed to screen the top drug candidates with the lowest binding energy (Supplementary Table 3). Among top 10 metabolites (Table 4), Eliglustat (DB09039) was found superior in terms of free binding energy for both protein targets, followed by Simvastatin (DB09039) and Hydroxocobalamin (DB00200) for VIBPA Type II secretion system protein L (Q87TC9) and VIBPA Putative fimbrial protein Z (Q87I65) respectively. ADME analysis was performed to get an insight into how the predicted pharmaceuticals will interact with the body as a whole (Table 5).

Screening of novel outer membrane proteins for vaccine construction

From the 25 novel outer membrane proteins (Supplementary file 14) designated as Set 11, two were selected based on the highest antigenicity score and human microbiome analysis to develop a novel chimeric peptide vaccine against *V. parahemolyticus* (Table 6). The schematic diagram summarizing the protocol over *in silico* vaccinomics strategy has been elucidated in Fig. 1. Sensor histidine protein kinase (Q87HJ8) and flagellar hook-associated protein (Q87JH9) possessed better antigenicity (0.64 and 0.53 respectively) while showed less percentage similarity (<45% and <41% respectively) when compared with gut microbiome data (Supplementary Table 4).

T-cell epitope prediction, transmembrane topology screening and antigenicity analysis

A plethora of CTL and HTL epitopes were identified for both proteins that can bind to the different large number of HLA-A and HLA-B alleles using MHC class-I and MHC class II binding predictions of IEDB (Supplementary File 15). Top epitopes (MHC-I and MHC-II binding peptides) for both proteins having the capacity to elicit strong T-cell responses were selected as putative T cell epitope candidates according to their topology screening by TMHMM and antigenic scoring (AS) by Vaxijen server (Supplementary File 16).

Population coverage, allergenicity, toxicity and conservancy analysis

Two different population coverages were calculated from CTL and HTL populations for MHC class I and MHC class II restricted peptides, respectively (Fig. 4). Epitopes, found to be non-allergen for humans, were identified according to the allergenicity assessment via four servers (Supplementary File 17). However, epitopes predicted as a toxin was removed from the proposed list of epitopes. Several epitope candidates from both proteins were found to be highly conserved within different strains of *V. parahemolyticus* with maximum conservancy level of 99% for histidine protein kinase and 100% for flagellar hook-associated protein respectively (Supplementary Table 5). Top 3 epitopes (CTL and HTL) for each protein were considered based on the above-mentioned parameters to design the final vaccine construct (Table 7).

Prediction of 3D structures for superior epitopes and analysis of molecular docking

The epitopes, showing conservancy pattern at a biologically significant level, were only allowed for further docking analysis. 3D structures were predicted for top epitopes (6 from Flagellar hook-associated protein and six from sensor histidine protein kinase) to analyze their interactions with different HLA alleles. The PEP-FOLD3 server modeled five 3D structures for each epitope, and the best one was identified for docking study. The result showed that 'AILLFPFAL' epitope of Flagellar hook-associated protein was superior in terms of free binding energy while interacted with HLA-A* 11:01 (−8.3 kcal/mol). Demonstrated energy was −9.1 kcal/mol for epitope 'GGRHNNLDL' of Sensor histidine protein kinase (Table 8).

Identification of B-Cell epitope

B-cell epitopes of both proteins were generated using six different algorithms from IEDB (Supplementary Fig. 1 and Supplementary Fig. 2). The epitopes were further investigated to reveal their non-allergenicity pattern, and the top one epitope from each prediction was selected for vaccine construction (Supplementary Table 6).

Epitope cluster analysis and vaccine construction

The construction of vaccine protein was based on identifying larger cassettes containing multiple epitopes. Epitope cluster analysis tool from IEDB predicted 21 epitope clusters among the top epitopes (6 CTL, 6 HTL epitopes, and 12 BCL epitopes) proposed in table 8 and supplementary table 2. Each vaccine construct was occupied by a protein adjuvant, PADRE peptide sequence, T-cell and B-cell epitopes with their respective linkers (Supplementary Table 7). Constructs V1, V2 and V3 were 370, 455 and 484 residues long, respectively. PADRE sequence was used to enhance the potency and efficacy of the peptide vaccine.

Allergenicity, antigenicity and solubility prediction of different vaccine constructs

Results revealed V1 as the most potent vaccine candidate with better antigenic nature (1.18) and non-allergic behavior that can elicit a strong immune response (Supplementary Table 7). All three constructs showed solubility above the threshold value (0.45). Again, construct V1 was superior in terms of solubility potential. The surface distribution of charge, hydrophobicity and stability were calculated at 91 different combinations of pH and ionic strength (Fig. 5).

Physicochemical characterization and secondary structure analysis

The molecular weight of the designed construct V1 was 39.45 kDa. The theoretical pI 9.95 implied that the protein would have a net negative charge above this pI and vice versa. At 0.1% absorption, the extinction coefficient was 26,930, while assuming all cysteine residues reduced. The estimated half-life was predicted to be >10 h in *E. coli* in vivo, whereas 1 h within mammalian reticulocytes in vitro. Hydrophilic behavior and thermostability of the protein were represented by the GRAVY value and aliphatic index that were−0.510 and 67.62, respectively. Instability index (37.49) and various physicochemical features classified the protein as a stable one with the capacity to induce a robust immunogenic reaction in the body. The predicted secondary structure confirmed to have 35.6% alpha helix, 11.89% sheet and 52.43% coil region (Supplementary Fig. 3). Around 34.59% polar, 16.21% hydrophobic and 9.46% aromatic regions were identified in the structure (Fig. 5).

Tertiary structure prediction, refinement, validation and disulfide engineering of vaccine construct

I-TASSER predicted five models for each proposed vaccine candidates, which were ranked based on cluster size. Ten best templates (with the highest Z-score) selected from the LOMETS threading programs were used to predict the tertiary structures. Homology modeling was performed by using 1kj6 from RCSB Protein Data Bank) as a best suited template for Vaccine protein V1. Results showed that model 1 had the highest C-Score of -2.11 while the estimated TM-score and RMSD were 0.46±0.15 and 11.6±4.5Å (Fig. 6). After refinement, 88.3% and 98.1% residues were in the favored and allowed region revealed by Ramachandran plot analysis (Fig. 6). The modeled tertiary structure of designed construct V2 and V3 have been shown in Supplementary Fig. 4. A total of 22 pairs of amino acid residues were identified with the potential to form disulfide bonds by DbD2 server. However, only two pairs (i.e., ARG 82-Gly 85, Lys 347-Thr 350) were compatible with

disulfide bond formation considering the energy, chi3 and B-factor parameter (Supplementary Fig. 5). All these residues were replaced with a cysteine residue.

Protein-protein docking and molecular dynamics simulation

Docking study was conducted between three vaccine constructs (i.e., V1, V2, V3) and different HLA alleles. Construct V1 showed biologically significant results and found to be superior in terms of free binding energy (Supplementary Table 8). Besides, the binding affinity of the predicted vaccine and TLR1-2 heterodimer complex was also analyzed. The 3D structure of human TLR-1/2 heterodimer was retrieved from the RCSB protein data bank. ClusPro generated thirty protein-ligand complexes (clusters) as output along with respective free binding energy. The lowest energy was −1257.9 for cluster 1 (Fig. 7). FireDock output refinement of the PatchDock server showed the lowest global energy of −7.08 for solution 5. Normal mode analysis allowed the demonstration of large scale mobility and the stability of proteins. The analysis was performed based on the internal coordinates of the protein-protein complex. In the 3D model, the direction of each residue was given by arrows, and the length of the line represented the extent of mobility (Fig. 8A). The eigenvalue found for the complex was 2.4784e−05 (Fig. 8B). The vaccine protein V1 and TLR1-2 heterodimers were oriented towards each other. The B-factor values deduced from normal mode analysis was analogous to RMS (Fig. 8C). Hinges in the chain indicated the probable deformability of the complex measured by the contortion of each residue (Fig. 8D). The variance associated with each normal mode was inversely linked to the eigenvalue. Covariance matrix explained the coupling between pairs of residues was correlated, uncorrelated, or anti-correlated motions were represented via red, white and blue colors, respectively (Fig. 8E). The result also generated an elastic network model (Fig. 8F) that identified the pairs of atoms connected via springs. Each dot in the diagram was indicated one spring between the corresponding pair of atoms and colored based on the degree of stiffness.

Codon adaptation, in silico cloning and similarity analysis with human proteins

E. coli strain K12 was selected as the host for the cloning purpose of the vaccine construct V1. Vaccine protein V1 was transcribed reversely, where the Codon Adaptation Index (CAI) was

found 0.994, and the GC content of the optimized codons (50.55%) was also significant. The construct did not hold restriction sites for ApaI and BglI, which ensured its safety for cloning purposes. The optimized codons were incorporated into the pET28a(+) vector along with ApaI and BglI restriction sites. A clone of 5634 base pair was obtained, including the 1118 bp desired sequence and the rest belonging to the vector. The desired region was shown in red color in between the pET28a(+) vector sequence (Fig. 9). Sequence similarity analysis of the proposed vaccine with human proteins revealed that there was no similarity between predicted vaccine constructs and human proteins.

Discussion

Due to severe effects on human health (Velazquez-Roman et al., 2014; Wu et al., 2014), the emergence of rapid antibiotic resistance (Golkar et al., 2014) and also having economic importance for substantially impairing the aquaculture production (Tang et al., 2014), it has become an urgent necessity to develop effective drug targets and vaccine candidates against *Vibrio parahaemolyticus.* Different computational approaches are now being widely practiced to identify proteins those are essential for the survival of the pathogen and not involved in the metabolic pathways of the host, thereby choosing the proteins associated only in the metabolic pathways of the pathogen is important (Judson and Mekalanos, 2000; Hossain et al., 2013). Essential proteins are most promising for new antibacterial drug targets since most antibiotics are designed to bind essential gene products (Zhang et al., 2004). Here, subtractive genome approaches (removal of paralogous proteins, identification of non-homologous proteins against the host, identification of essential proteins and metabolic pathways analysis of the pathogen), and vaccinomics strategy were employed for identifying novel drug and vaccine molecules through the comprehensive proteome exploration of *Vibrio parahaemolyticus* genome.

The complete proteome of *V. parahaemolyticus* (4822 proteins) was retrieved from the NCBI database, and the homologous proteins were removed based on their identity with human proteins. Proteins encoded by essential genes and unique to an organism can be considered as species-specific drug targets (Mondal et al., 2015), as they play vital roles in its metabolism. The study revealed 96 unique, essential proteins (Set5) of *V. parahaemolyticus,* which can be considered as suitable drug targets for combating *V. parahaemolyticus* infections. Among the unique proteins,

55 proteins were druggable and can be targeted using existing drugs (92) that are already approved and available in the market (Supplementary Table 1). In the case of a broad-spectrum drug, for avoiding mutational changes as well as the emergence of resistant bacteria, the DrugBank databases were screened, which contains entries for 2556 approved small molecule drugs, 962 approved biotech drugs, 112 nutraceuticals and over 5125 experimental drugs. A total of 41 proteins of *V. parahaemolyticus* showed no similarity after passing through the DrugBank database and listed for the prediction of novel drug targets and vaccine candidates (set 6). To avoid severe cross-reaction and toxic effects in human, identification of nonhomologous proteins to essential human proteins (referred to as 'anti-targets') was a crucial step considered in this study. However, the identified novel drug targets (41) showed no evidence of similarity with the 'anti-targets'. Although both cytoplasmic and membrane proteins serve the purpose as therapeutic targets (Michael et al., 2014), membrane proteins are best suited for vaccine candidates (Baliga et al., 2018; Hasan et al., 2019a). Hence, in this study, membrane proteins (25) were used for vaccine construction, whereas cytoplasmic proteins (16) were proposed as suitable drug targets. Targeting human microbiome non-homology proteins is suitable since drugs or vaccines designed and administered for these targets will be less harmful to other commensal microbial strains. Among the novel cytoplasmic proteins (16), only the proteins (9) conferring <45% similarity with human microbiota were retained. TheVFDB (virulence factor database) analysis studies confirmed that 'VIBPA Type II secretion system protein L (Q87TC9)' and 'VIBPA Putative fimbrial protein Z (Q87I65)' were associated with virulence in the host (Set 10). The protein-protein interaction studies also strengthened the superiority of these two proteins as suitable drug targets (Table 4).

Molecular docking of 350 human metabolites against 'VIBPA Type II secretion system protein L' and 'VIBPA Putative fimbrial protein Z' was conducted to screen superior drug molecules (Supplementary Table 2). The study revealed that 'Eliglustat (DB09039)' was the top drug molecules for both protein targets in terms of free binding energy (Table 5). Therefore, it can be suggested as a suitable drug to treat infections caused by *V. parahaemolyticus*. Moreover, drug profiling (Physicochemical parameters, Lipophilicity, Pharmacokinetics, Water Solubility, Druglikeness, Medicinal Chemistry) of 'Eliglustat (DB09039)' along with other top candidates, i.e., 'Simvastatin (DB09039)' and 'Hydroxocobalamin (DB00200)' were also performed through ADME analysis (Table 5).

Several advantages help the researchers to select membrane proteins both as drug and vaccine candidates as their functions can be easily studied through computer-based approaches than wet-lab process (Hasan et al., 2019a; Hasan et al., 2019b). In this study, two vaccine targets, 'Sensor histidine protein kinase UhpB (Q87HJ8)' and 'Flagellar hook-associated protein (Q87JH9)' were selected after screening the novel outer-membrane proteins (25) based on their antigenicity score and human microbiome non-homology analysis (Table 6). Both the proteins further analyzed to design a potent, highly immunogenic vaccine candidate against *V. parahaemolyticus.* Numerous antigenic epitopes were generated which were investigated extensively for antigenicity, allergenicity, toxicity, conservancy and other physiochemical properties using a number of bioinformatics tools and software. The final vaccine constructs were designed with the help of different adjuvants and amino acid linkers (Solanki and Tiwari, 2018). It has been reported that the PADRE sequence reduces the polymorphism of HLA molecules in the population (Ghaffari-Nazari et al., 2013; Hasan et al., 2019b). Linkers in vaccines also enhanced the immunogenicity of the vaccines in previous studies (Yang et al., 2015; Hasan et al., 2019c). Therefore, all the important that could induce the immunogenicity of the designed vaccine constructs were taken. Also, disulfide engineering was employed to enhance the stability of the designed vaccine. The purpose of the molecular docking analysis was to show the proposed epitopes could interact with at least one MHC molecule at minimum binding energy. Therefore, it was done to explore the binding affinity of promiscuous epitopes with different HLA alleles including HLA-DRB1*03:01 (1A6A), (HLA-DRB5*01:01 (1H15), HLA-DRB3*01:01 (2Q6W), HLA-DRB1*04:01 (2SEB), HLA-DRB1*01:01 (2FSE), and HLA-DRB3*02:02 (3C5J). The OmpU, one of the major outer membrane porins of *V. parahaemolyticus*, is recognized by the Toll-like receptor 1/2 (TLR1/2) heterodimer in THP-1 monocytes (Gulati et al., 2019). So, a docking study was also performed to analyze the affinity between the designed construct and human TLR1/2 heterodimer. The vaccine receptor complex showed deformability at a minimum level, which also strengthened our prediction. Finally, the optimized codons of the designed construct been cloned into the pET28a(+) vector of *E. coli* strain K12.

The idea of subtractive genomic analysis using various bioinformatics tools has brought a revolution in the drug discovery process. The present study will help to develop novel therapeutics and preventive measures against *V. parahaemolyticus*, thereby help to reduce the mortality and

morbidity caused by it. However, further in vivo trials using model organisms are highly recommended to validate our prediction.

Materials and Methods

The whole proteome of *V. parahemolyticus* was analyzed according to subtractive genomic approach to recognize novel drug targets as well as vaccine candidates. The overall workflow for subtractive proteomic analysis and vaccinomics approach has been illustrated in Fig .1 and Fig. 2, respectively.

Retrieval of complete proteome and identification of essential proteins

The whole proteome of *V. parahemolyticus* strain O3:K6 was retrieved from NCBI Genome database. Paralogous sequences were excluded from the proteome of *V. parahemolyticus* by using CD-HIT (Li and Godzik, 2006). With a cutoff score of 0.6, proteins with more than 60% identity were excluded. Remaining proteins were subjected to BLASTp against *H. sapiens* human Refseq proteome in 'Ensemble Genome Database 92' using threshold expectation value (E- value) 10^{-3} as the parameter. Proteins were assumed as homologous were excluded if any significant hit above the threshold value 10^{-4} was found. The remaining non-homologous proteins were subjected to the Database of Essential Genes (DEG) (Zhang et al., 2004; Luo, 2013). Proteins hit with expectation value $\leq$10-100, identity $\geq$ 25% were listed for metabolic pathway analysis considering as essential non-homologous proteins of *V. parahemolyticus*.

Analysis of metabolic pathways

Kyoto Encyclopedia of Genes and Genomes which contains complete metabolic pathways present in living organisms (Moriya et al., 2007). Metabolic pathways of *V. parahemolyticus* were analyzed against the human metabolic pathways through the KEGG server. All metabolic pathways present in the pathogen (*V. parahemolyticus*) and host (*H. sapiens*) were collected from the KEGG PATHWAY database using three letters KEGG organism code 'vpa' and 'has' respectively. A comparison was made in order to recognize the unique metabolic pathways only present in the *V. parahemolyticus*, while the remaining pathways of the pathogen were grouped as

a common one. Identified host non-homologous, essential proteins of *V. parahemolyticus* were subjected to BLASTp through the KAAS server at KEEG. Proteins present only in the unique metabolic pathways of the pathogen were listed for further analysis.

Druggability analysis and identification of novel drug targets

A 'druggable' target needs to have the potentiality to bind to the drugs and drug-like molecules with high affinity. Shortlisted unique proteins were screened through the database of DrugBank 5.1.0 (Wishart et al., 2017) using default parameters to identify both druggable proteins and novel therapeutic targets.

'Anti-target' analysis and prediction of subcellular localization

This analysis was performed to avoid any kind of cross-reactivity, and toxic effects due to docking between the drugs administered for the pathogen and the host 'anti-targets'.'Anti-targets' are gene products that show cross-reactivity with administered therapeutics. Novel drug targets were subjected to BLASTp analysis in the NCBI blast program against these human 'anti-targets' setting an E-value <0.005, query length >30%, identity <25% as parameters. Proteins were showing a <25% identity that was listed for subcellular localization analysis. Besides, proteins functioning in cytoplasm can be used as putative drug targets, while surface membrane proteins can be considered both as drug targets and vaccine candidates. PSORTb v3.0.2 (http://www.psort.org/psortb/index.html), CELLO v.2.5 (http://cello.life.nctu.edu.tw/), ngLOC servers were used to predict subcellular localization of shortlisted pathogen-specific essential proteins.

Human microbiome non-homology analysis

Both membrane and cytoplasmic proteins were subjected to BLASTp through NCBI protein blast server against the dataset present in the Human Microbiome Project server (https://www.hmpdacc.org/hmp/) "(BioProject-43021)" (Turnbaugh et al., 2007) with a cutoff

score 0.005. Membrane proteins showing <45% similarity were selected for vaccine candidacy, whereas cytoplasmic proteins showing <45% similarity were selected for protein-protein interaction analysis.

Analysis of virulence factors (VF's) and protein-protein interactions studies (PPIs)

Virulence factors are responsible for modulating or degrading host defense mechanisms by bacteria. Novel cytoplasmic proteins with the least similarity with the human microbiome were subjected to BLASTp search against the database of protein sequences from the VFDB core dataset (Chen et al., 2005) with default hit with cut-off bit score >100, and E-value was 0.0001. The protein-protein interactions studies (PPIs) of selected shortlisted proteins were predicted using STRING v10.5 (Szklarczyk et al., 2018). PPIs with a high confidence score (≥90%) were considered to avoid false-positive results. Only characterized proteins were subjected to BLASTp.

Screening of drug molecules against novel cytoplasmic proteins

All the pharmaco-metabolites reported in the Human Metabolites Database (www.hmdb.ca) were used for the screening of suitable drugs. Molecular docking was performed against predicted drug targets (novel cytoplasmic proteins) by using AutoDock Vina tools (Trott and Olson, 2010). The size of the grid box was set to 54 A° x 74 A° x 126 A° (x, y and z) and 65A° x 85 A° x 65 A° (x, y and z) with 1 A° spacing between the grid points for two cytoplasmic therapeutic target proteins (Q87TC9 and Q87165 respectively).

Screening of novel outer membrane proteins for vaccine construction

The VaxiJen v2.0 (http://www.ddg-pharmfac.net/vaxijen/) was used for the investigation of protein immunogenicity to find the most potent antigenic outer membrane proteins (Doytchinova and Flower, 2007a). Proteins were prioritized based on their antigenic score (threshold value 0.4) and sequence similarity with human microbiota.

T-cell epitope prediction, transmembrane topology screening and antigenicity analysis

MHC-I (http://tools.iedb.org/mhci/) and MHC-II prediction tool (http://tools.iedb.org/mhcii/) prediction tool of the Immune Epitope Database were used to predict the MHC-I binding and MHC-II binding peptides, respectively. To predict the transmembrane helices in proteins (Krogh et al., 2001) and to determine epitope antigenicity (Doytchinova and Flower, 2007b), TMHMM (http://www.cbs.dtu.dk/services/TMHMM/) and VaxiJen v2.0 server (http://www.ddg-pharmfac.net/vaxijen/) were utilized.

Population coverage, allergenicity, toxicity and conservancy analysis

Population coverage for each epitope was analyzed by the IEDB population coverage calculation tool (http://tools.iedb.org/population/) (Vita et al., 2014). The most potent antigenic epitopes were selected and allowed for determining the allergenicity pattern via four servers named AllergenFP (Dimitrov et al., 2014), AllerTOP (http://www.ddg-pharmfac.net/AllerTop/) (Dimitrov et al., 2013), Allermatch (http://www.allermatch.org/allermatch.py/form) (Fiers et al., 2004) and Allergen Online (Goodman et al., 2016). Moreover, the ToxinPred server predicted the toxicity level of the proposed epitopes (http://crdd.osdd.net/raghava/toxinpred/) (Gupta et al., 2013). The conservancy level determines the efficacy of epitope candidates to confer broad-spectrum immunity. For revealing the conservancy pattern, homologous sequence sets of the selected antigenic proteins were retrieved from the NCBI database by using the BLASTp tool. Further, the epitope conservancy analysis tool (http://tools.iedb.org/conservancy/) at IEDB was selected for the analysis of the conservancy pattern.

Prediction of 3D structures for superior epitopes and analysis of molecular docking

Top-ranked epitopes were subjected to the PEP-FOLD server to predict peptide structures (Wang et al., 2011). Depending on the available structures deposited in Protein Data Bank (PDB) database, HLA-A*11:01 and HLA-DRB1*04:01 were selected for docking analysis with MHC

class I and class II binding epitopes respectively. MGLTools were used to visualize and analyze the molecular structures of biological compounds (Sanner, 1999). The grid box was set to 28 A°, 18 A°, 20 A° (x, y and z) with a default value of 1.0 A° spacing by AutodockVina at 1.00- °A spacing. The exhaustiveness parameter was kept at 8.00, and the number of outputs was set at 10 (Morris et al., 2009). Output PDBQT files were converted in PDB format using Open Babel. The docking interaction was visualized with the PyMOL molecular graphics system (https://www.pymol.org/).

Identification of B-Cell epitope

B cell epitopes were predicted for both proteins to find the potential antigens that would interact with B lymphocytes and initiate the immune response. Several tools from IEDB i.e. Kolaskar and Tongaonkar antigenicity scale (Kolaskar and Tongaonkar, 1990), Karplus and Schulz flexibility prediction (Karplus and Schulz, 1985), Bepipred linear epitope prediction analysis (Jespersen et al., 2017), Emini surface accessibility prediction (Emini et al., 1985), Parker hydrophilicity prediction (Parker et al., 1986) and Chou and Fasman beta-turn prediction (Chou and Fasman, 1978) were used to identify the B cell antigenicity depending on six different algorithms.

Epitope cluster analysis and vaccine construction

Epitope cluster analysis tool from IEDB was used to identify the epitope clusters with overlapping peptides for both proteins using the top CTL, HTL and BCL epitopes as input. The identified clusters and singletons were further utilized to design construct. Vaccine sequences started with an adjuvant followed by the top CTL epitopes, top HTL epitopes and BCL epitopes respectively for both proteins. Three vaccine constructs i.e. V1, V2 and V3, each associated with different adjuvants including beta-defensin (a 45 mer peptide), L7/L12 ribosomal protein and HABA protein (*M. tuberculosis*, accession number: AGV15514.1) (Rana and Akhter, 2016) were constructed. PADRE sequence and different linkers, for instance, EAAAK, GGGS, GPGPG and KK linkers, were also used to construct effective vaccine molecules.

Allergenicity, antigenicity and solubility prediction of different vaccine constructs

The AlgPred v.2.0 (Saha and Raghava, 2006) and AllerTOP v.2.0 (Dimitrov et al., 2013) servers were utilized to predict the non-allergic behavior of the vaccine constructs. For proposing the superior vaccine candidate, the VaxiJen v2.0 server (Doytchinova and Flower, 2007b) was utilized. The probable antigenicity of the constructs was determined through an alignment-independent algorithm. Protein-sol software (Hebditch et al., 2017) predicted the solubility score of the proposed vaccines.

Physicochemical characterization and secondary structure analysis

The ProtParam, a tool from Expasy's server (http://expasy.org/cgi-bin/protpraram)(Gasteiger et al., 2003; Hasan et al., 2015) was used to characterize the vaccine proteins functionally – including molecular weight, isoelectric pH, aliphatic index, hydropathicity, instability index, GRAVY values and estimated half-life and other physicochemical properties were investigated. The PSIPRED v3.3 (Kosciolek and Jones, 2014; Packer, 2012) were used to predict the alpha helix, beta sheet and coil structure of the vaccine protein. The polar, nonpolar and aromatic regions were also determined.

Tertiary structure prediction, refinement, validation and disulfide engineering of vaccine construct

The I-TASER server (Yang et al., 2015) was employed for determining the 3D structure of designed vaccine constructs based on the degree of similarity between the target protein and available template structure from PDB. Refinement was performed using ModRefiner (Xu and Zhang, 2011). The refined protein structure was validated through the Ramachandran plot assessment by the MolProbity software (Chen, V.B. et al., 2010). Residues in the highly mobile region of the protein exhibit the potential to be mutated with cysteine. Pairs of residues with proper geometry and the ability to form a disulfide bond were detected by the DbD2 server to perform disulfide engineering (Craig and Dombkowski, 2013). The value of chi3 considered for the residue screening was between −87 to +97 while the energy considered was<2.5.

Protein-protein docking and molecular dynamics simulation

The binding affinity of the vaccine constructs with different HLA alleles and human immune receptors, ClusPro 2.0 (Comeau et al., 2004), hdoc (Macalino et al., 2018) and PatchDock server (Schneidman-Duhovny et al., 2005) were applied. Desirable complexes were identified according to better electrostatic interaction and free binding energy following refinement via the FireDock server (Mashiach et al., 2008). The iMODS server was used to explain the collective motion of proteins via analysis of normal modes (NMA) in internal coordinates (Lopez-Blanco et al., 2014). Essential dynamics is a powerful tool and alternative to the costly atomistic simulation that can be compared to the normal modes of proteins to determine their stability (Aalten et al., 1997; Wuthrich et al., 1980; Cui and Bahar, 2007). The server predicted the direction and magnitude of the immanent motions of the complex in terms of deformability, eigenvalues, B-factors and covariance. The structural dynamics of the protein-protein complex was investigated (Prabhakar et al., 2016).

Codon adaptation, in silico cloning and similarity analysis with human proteins

A codon adaptation tool (JCAT) was used to adapt the codon usage to the well-characterized prokaryotic organisms for accelerating the expression rate in it. Rho-independent transcription termination, prokaryote ribosome binding site and cleavage sites of restriction enzyme ApaI and BglI were avoided while using the server (Grote et al., 2005). The optimized sequence of vaccine protein V1 was reversed, followed by conjugation with ApaI and BglI restriction site at the N-terminal and C-terminal sites, respectively. SnapGene (Solanki and Tiwari, 2018) restriction cloning module was used to insert the adapted sequence into the pET28a(+) vector between ApaI (1334) and BglI (2452). At last, human sequence similarity analysis of the proposed vaccine with human proteins was done by using NCBI protein-protein Blast (https://blast.ncbi.nlm.nih.gov/Blast.cgi), and here blast was done against Homo sapiens (taxid: 9606) dataset.

Funding

The authors received no direct funding for this research.

Author contributions

Mahmudul Hasan, Conceptualization, Data curation, Formal analysis, Investigation, Visualization, Methodology, Manuscript- original draft, review and editing; Kazi Faizul Azim, Abdus Shukur Imran and Ishtiak Malique Chowdhury, Resources, Data curation, Formal analysis, Validation, Investigation, Visualization, Manuscript writing; Shah Rucksana Akhter Urme, Md Sorwer Alam Parvez and Md Tahsin Khan, Software, Formal analysis, Validation, Investigation, Visualization, Manuscript writing; Md Bashir Uddin and Syed Sayeem Uddin Ahmed, Conceptualization, Resources, Data curation, Software, Analysis, Validation, Visualization, Methodology, Supervision, Manuscript- original draft, review and editing.

Declaration of interests

The authors declare that they have no known competing financial interests or personal relationships that could have appeared to influence the work reported in this paper.

Data availability

All data generated and analysed during this study is included in the main manuscript or supplementary files.

References

Tang, K. F. & Lightner, D. V. Homologues of insecticidal toxin complex genes within a genomic island in the marine bacterium *Vibrio parahaemolyticus*. *FEMS Microbiol. Lett.* **361**, 34–42 (2014).

Ghenem, L., Elhadi, N., Alzahrani, F. & Nishibuchi, M. Vibrio Parahaemolyticus: A review on distribution, pathogenesis, virulence determinants and epidemiology. *Saudi. J. Med. Med. Sci.* ***5***, 93 (2017).

Chen, A. J., Hasan, N. A., Haley, B. J., Taviani, E., Tarnowski, M., Brohawn, K., Johnson, C. N., Colwell, R. R. & Huq, A. Characterization of pathogenic Vibrio parahaemolyticus from the Chesapeake Bay, Maryland. *Front. Microbial*. ***8***, 2460 (2017).

Letchumanan, V., Chan K. G. & Lee L. H. *Vibrio parahaemolyticus*: A review on the pathogenesis, prevalence, and advance molecular identification techniques. *Front. Microbiol.* **5**, 705 (2014).

Rico, A., Satapornvanit, K., Haque, M. M., Min, J., Nguyen, P. T. & Telfer, T. Use of chemicals and biological products in Asian aquaculture and their potential environmental risks: acritical review. *Rev. Aqua.* **4**, 75–93 (2012).

Bondad-Reantaso, M. G., Subasinghe, R. P., Arthur, J. R., Ogawa, K., Chinabut, S. & Adlard, R. Disease and healt hman age mentin Asian aquaculture. Vet. Parasitol. **132**, 249–272 (2005).

Food and Agriculture Organization [FAO]. (2016). Drivers, Dynamics and Epidemiology of Antimicrobial Resistance in Animal Production. Available at: http://www.fao.org/3/a-i6209e.pdf

Food and Agriculture Organization [FAO] (2015). The FAO Action Plan on Antimicrobial Resistance 2016–2020. Rome: Food and Agriculture Organization of the United Nations.

Tendencia, E. A., & de la Peña, L. D. Antibiotic resistance of bacteria from shrimp ponds. *Aquaculture*, **195**, 193–204 (2001).

Vaseeharan, B., Ramasamy, P., Murugan, T. & Chen, J. C. In vitro susceptibility of antibiotics against Vibrio spp. and Aeromonas spp. Isolated from Penaeus monodon hatcheries ponds. *Int. J. Antimicrob. Agents,* **26**, 285–291 (2005).

Han, F., Walker, R. D., Janes, M. E., Prinyawiwatkul, W. & Ge, B. Antimicrobial susceptibilities of Vibrio parahaemolyticus and Vibrio vulnificus isolates from Louisiana Gulf and retail raw oyster. *Appl. Environ. Microbiol.* **73**, 7096–7098 (2007).

Yang, Y., Xie, J., Li, H., Tan, S., Chen, Y. & Yu, H. Prevalence, antibiotic susceptibility and diversity of Vibrio parahaemolyticus isolates in seafood from South China. *Front. Microbiol.* ***8***, 2566 (2017).

Lesley, M. B., Velnetti, L., Cheah, Y. K., Son, R., Kasing, A., Samuel, L., et al. Antibiotic resistance and plasmid profiling of Vibrio parahaemolyticus isolated from cockles (Anadara granosa) at Tanjung Karang, Kuala Selangor. *Int. Food Res. J.* **18**, 1183–1188 (2011).

Noorlis, A., Ghazali, F. M., Cheah, Y. K., Tuan Zainazor, T. C., Wong, W. C., Tunung, R., Pui, C. F., Nishibuchi, M., Nakaguchi, Y. & Son, R. Antibiotic resistance and biosafety of Vibrio cholerae and Vibrio parahaemolyticus from freshwater ish at retail level. *Int. Food Res. J.* **18**, 1523–1530 (2011).

Osunla, C. & Okoh, A. Vibrio pathogens: A public health concern in rural water resources in sub-Saharan Africa. *Int. J. Environ. Res. Public Health*, ***14***, 1188 (2017).

Jung, S. W. A foodborne outbreak of gastroenteritis caused by Vibrio parahaemolyticus associated with cross-contamination from squid in Korea. *Epidemiol. Health* 40 (2018).

Liu, Y., Tam, Y. H., Yuan, J., Chen, F., Cai, W., Liu, J., Ma, X., Xie, C., Zheng, C., Zhuo, L. & Cao, X. A foodborne outbreak of gastroenteritis caused by Vibrio parahaemolyticus and norovirus through non-seafood vehicle. *PloS one*, **10**, e0137848 (2015).

Jang, H. G., Kim, N. H., Choi, Y. M. & Rhee, M.S. Microbiological quality and risk factors related to sandwiches served in bakeries, cafés, and sandwich bars in South Korea. *J. Food Prot.* **76**, 231-8 (2013).

Daniels, N. A., MacKinnon, L., Bishop, R., Altekruse, S., Ray, B., Hammond, R. M., Slutsker, L., et al. Vibrio parahaemolyticus infections in the United States, 1973–1998. *The J. of infect. dis.* **181**, 1661-1666 (2000).

Alam, M. J., Tomochika, K. I., Miyoshi, S. I. & Shinoda, S. Environmental investigation of potentially pathogenic *Vibrio parahaemolyticus* in the Seto-Inland Sea, Japan. *FEMS Microbiol. Lett.* **208**, 83–87 (2002).

Wang, L., Zhao, X., Chu, J., Li, Y., Li, Y., Li, C., Xu, Z. & Zhong, Q. Application of an improved loop-mediated isothermal amplification detection of Vibrio parahaemolyticus from various seafood samples. *African J. of Microbiol. Res.* **5**, 5765-71 (2011).

Wu, Y., Wen, J., Ma, Y., Ma, X. & Chen, Y. Epidemiology of foodborne disease out breaks caused by *Vibrio parahaemolyticus*, China, 2003–2008. *Food Cont.* **46**, 197–202 (2014).

Liu, X. M., Chen, Y., Fan, Y. X. & Wang, M. Q. Food borne diseases occurred in 2003--report of the National Foodborne Diseases Surveillance System, China. *J. of hygiene res.* **35**, 201-4 (2006).

Nair, G. B., Ramamurthy, T., Bhattacharya, S. K., Dutta, B., Takeda, Y. & Sack, D. A. Global dissemination of Vibrio parahaemolyticus serotype O3: K6 and its serovariants. *Clinical microbial. reviews*. **20**, 39-48 (2007).

Chao, G., Wang, F., Zhou, X., Jiao, X., Huang, J., Pan, Z., Zhou, L. & Qian, X. Origin of Vibrio parahaemolyticus O3: K6 pandemic clone. *Int. J. Food Microbiol*. 145, 459-63 (2011).

Kaysner, C. A. & De Paola, A. "Vibrio," in Compendium of Methods for the Microbiological Examination of Foods (ed. Downes, F. P. & Ito, K.) 405–420 (Washington, DC: American Public Health Association, 2001).

Newton, A., Kendall, M., Vugia, D. J., Henao, O. L. & Mahon, B. E. Increasing rates of *Vibrio sisinthe* UnitedStates, 1996–2010: review of surveillance data from 2 systems. Clin. *Infect. Dis.* **54**, S391–S395 (2012).

Scallan, E., Hoekstra, R. M., Angulo, F. J., Tauxe, R. V., Widdowson, M. A. & Roy, S. L. Foodborne illness acquired in the United States– major pathogens. *Emerg. Infect. Dis.* **17**, 7–15 (2011).

Huang, J. Y., Henao, O. L., Griffin, P. M., Vugia, D. J., Cronquist, A. B. & Hurd, S. Infection with pathogens transmitted commonly through food and the effect of increasing use of culture-independent diagnostic tests on surveillance – foodborne diseases active surveillance network, 10 U.S. sites, 2012-2015. *Morb. Mortal. Wkly. Rep.* **65**, 368–371 (2016).

Cruz, C. D., Hedderley, D. & Fletcher, G. C. *Vibrio parahaemolyticus* prevalence and distribution in New Zealand shellfish: along-termstudy. Appl. Environ. Microbiol. **81**, 2320-7 (2015)

Letchumanan, V., Yin, W. F., Lee, L. H. & Chan, K. G. Prevalence and antimicrobial susceptibility of Vibrio parahaemolyticus isolated from retail shrimps in Malaysia. *Front. Microbiol.* **6**, 33 (2015).

Gode-Potratz, C. J., Kustusch, R. J., Breheny, P. J., Weiss, D. S. & McCarter, L. L. Surface sensing in *Vibrio parahaemolyticus* triggers a programme of gene expression that promotes colonization and virulence. *Mol. Microbiol.* **79**, 240–263 (2011).

Peng, F. M., Jiang, D. Y., Ruan, H. H., Liu, H. Q. & Zhou, L. P. Pathogenic investigation on a food poisoning induced by *Vibrio parahaemolyticus*. *Prev. Med.* Trib. **16**, 746–747 (2010).

China Statistical Yearbook. Beijing: State Statistical Bureau (2012).

Rahimi, E., Ameri, M., Doosti, A. & Gholampour, A. R. Occurrence of toxigenic *Vibrio parahaemolyticus* strains in shrimp in Iran. *Foodborne Pathog.* Dis. **7**, 1107–1111 (2010).

Ham, H. & Orth, K. The role of type III secretion system 2 in Vibrio parahaemolyticus pathogenicity. *J. Microbiol.* **50**, 719-25 (2012).

Levin, R. E. Vibrio parahaemolyticus, a notably lethal human pathogen derived from seafood: A review of its pathogenicity, characteristics, subspecies characterization, and molecular methods of detection. *Food Biotechnol.* **20**, 93-128 (2006).

Ahmad, A., Brumble, L. & Maniaci, M. Vibrio parahaemolyticus induced necrotizing fasciitis: An atypical organism causing an unusual presentation. *Case Rep. Infect. Dis.* **2013**, 216854 (2013).

Zhang, L. & Orth, K. Virulence determinants for Vibrio parahaemolyticus infection. *Curr. Opin. Microbiol.* **16**, 70-7 (2013).

Xiao, J., Liu, L., Ke, Y., Li, X., Liu, Y., Pan, Y., Yan, S. & Wang, Y. Shrimp AHPND-causing plasmids encoding the PirAB toxins as mediated by pirAB-Tn903 are prevalent in various Vibrio species. *Sci. Rep*. **7**, 42177 (2017).

Yu, W. T., Jong, K. J., Lin, Y. R., Tsai, S. E., Tey, Y. H. & Wong, H. C. Prevalence of Vibrio parahaemolyticus in oyster and clam culturing environments in Taiwan. *Int. J. of food Microbiol.* **160**, 185-92 (2013).

Han, F., Walker, R. D., Janes, M. E., Prinyawiwatkul, W. & Ge, B. Antimicrobial susceptibilities of Vibrio parahaemolyticus and Vibrio vulnificus isolates from Louisiana Gulf and retail raw oysters. *Appl. Environ. Microbiol.*, ***73***,7096-7098 (2007).

Tan, L. T. H., Chan, K. G., Lee, L. H., & Goh, B. H. Streptomyces bacteria as potential probiotics in aquaculture. *Front. Microbiol.* **79**, 79 (2016).

Jun, J. W., Shin, T. H., Kim, J. H., Shin, S. P., Han, J. E., Heo, G. J., De Zoysa, M., Shin, G. W., Chai, J. Y. & Park, S. C. Bacteriophage therapy of a Vibrio parahaemolyticus infection caused by a multiple-antibiotic–resistant O3: K6 pandemic clinical strain. *J. Infect. Dis*. ***210***,72-78 (2014).

Lin, D. M., Koskella, B. and Lin, H. C. Phage therapy: An alternative to antibiotics in the age of multi-drug resistance. *World J. Gastrointest. Pharmacol. Ther.* ***8***, 162 (2017).

Sudha, S., Mridula, C., Silvester, R. & Hatha, A. A. M. Prevalence and antibiotic resistance of pathogenic Vibrios in shell fishes from Cochin market. *Indian J. Mar. Sci.* **43**, 815–824 (2014).

Lee, L. H., Ab Mutalib, N. S., Law, J. W. F., Wong, S. H. & Letchumanan, V. Discovery on antibiotic resistance patterns of Vibrio parahaemolyticus in Selangor reveals carbapenemase producing Vibrio parahaemolyticus in marine and freshwater fish. *Front. Microbiol.* ***9***, 2513 (2018).

Jun, J. W., Kim, J. H., Choresca, C. H., Shin, S. P., Han, J. E., Han, S. Y., et al. Isolation, molecular characterization and antibiotic susceptibility of Vibrio parahaemolyticus in Korean sea food. *Food borne Pathog. Dis.* **9**, 224–231 (2012).

Barh, D., Tiwari, S., Jain, N., Ali, A., Santos, A. R., Misra, A. N., Azevedo, V. & Kumar, A. In silico subtractive genomics for target identification in human bacterial pathogens. *Drug Develop. Res.* ***72*****(2)**, 162-177 (2011).

Azim, K. F., Hasan, M., Hossain, M. N., Somana, S. R., Hoque, S. F., Bappy, M. N., Chowdhury, A. T. & Lasker, T. Immunoinformatics approaches for designing a novel multi epitope peptide vaccine against human norovirus (Norwalk virus). *Infect. Genet. Evol*. **74**,103936 (2019).

Barh, D. & Kumar, A. In silico identification of candidate drug and vaccine targets from various pathways in *Neisseria gonorrhoeae*. *In silico boil*. **9**, 225-231 (2009).

Hosen, M. I., Tanmoy, A. M., Mahbuba, D. A., Salma, U., Nazim, M., Islam, M. T. & Akhteruzzaman, S. Application of a subtractive genomics approach for in silico identification and characterization of novel drug targets in *Mycobacterium tuberculosis* F11. *Interdisciplinary Sciences: Computational Life Sciences* **6**, 48-56 (2014).

Perumal, D., Lim, C. S., Sakharkar, K. R. & Sakharkar, M. K. Differential genome analyses of metabolic enzymes in *Pseudomonas aeruginosa* for drug target identification. *In silico boil*. **7**, 453-465 (2007).

Pagadala, N. S., Syed, K. & Tuszynski, J. Software for molecular docking: A review. *Biophys. Rev*. **9,** 91-102 (2017).

Wong, C. F. Flexible receptor docking for drug discovery. *Expert Opin. Drug Dis.* **10**, 1189-1200 (2015).

Ferreira, L. G., Dos Santos, R. N., Oliva, G. & Andricopulo, A. D. Molecular docking and structurebased drug design strategies. *Molecules*. **20,** 13384-13421 (2015).

Yuriev, E. & Ramsland, P. A. Latest developments in molecular docking: 2010–2011 in review. *J. Mol. Recognit*. **26**, 215-239 (2013).

Li, W. & Godzik, A. Cd-hit: a fast program for clustering and comparing large sets of protein or nucleotide sequences. *Bioinform.* **22**, 1658-1659 (2006).

Zhang, R., Ou, H. Y. & Zhang, C. T. DEG: a database of essential genes. *Nucleic acids res.* **32**, D271-D272 (2004).

Luo, H., Lin, Y., Gao, F., Zhang, C. T. & Zhang, R. DEG 10, an update of the database of essential genes that includes both protein-coding genes and noncoding genomic elements. *Nucleic acids res.* **42**, D574-D580 (2013).

Moriya, Y., Itoh, M., Okuda, S., Yoshizawa, A. C. & Kanehisa, M. KAAS: an automatic genome annotation and pathway reconstruction server. *Nucleic acids res*. **35**, W182-W185 (2007).

Wishart, D. S., Feunang, Y. D., Guo, A. C., Lo, E. J., Marcu, A., Grant, J. R., Sajed, T., Johnson, D., Li, C., Sayeeda, Z. & Assempour, N. DrugBank 5.0: a major update to the DrugBank database for 2018. *Nucleic acids res.* **46**, D1074-D1082 (2017).

Turnbaugh, P. J., Ley, R. E., Hamady, M., Fraser-Liggett, C. M., Knight, R. & Gordon, J. I. The human microbiome project. *Nature* **449**, 804 (2007).

Chen, L., Yang, J., Yu, J., Yao, Z., Sun, L., Shen, Y. & Jin, Q. VFDB: a reference database for bacterial virulence factors. *Nucleic acids res.* **33**, D325-D328 (2005).

Szklarczyk, D., Gable, A.L., Lyon, D., Junge, A., Wyder, S., Huerta-Cepas, J., Simonovic, M., Doncheva, N.T., Morris, J.H., Bork, P. & Jensen, L.J. STRING v11: protein–protein association networks with increased coverage, supporting functional discovery in genome-wide experimental datasets. *Nucleic acids res.* **47(D1)**, D607-D613 (2018).

Trott, O. & Olson, A.J. AutoDock Vina: improving the speed and accuracy of docking with a new scoring function, efficient optimization, and multithreading. *J Comput Chem*. **31**(**2**):455–461 (2010).

Doytchinova, I.A., Flower, Darren R. Identifying candidate subunit vaccines using an alignment-independent method based on principal amino acid properties. *Vaccine* **25**, 856–866 (2007).

Krogh, A., Larsson, B., Von Heijne, G. & Sonnhammer, E. L. Predicting transmembrane protein topology with a hidden markov model: application to complete genomes. *J. Mol. Biol.* **305**, 567–580 (2001).

Vita, R., Overton, J. A., Greenbaum, J. A., Ponomarenko, J., Clark, J. D. & Cantrell, J. R. The immune epitope database (IEDB) 3.0. *Nucleic Acids Res.* **43**, D405–D412 (2014).

Dimitrov, I., Bangov, I., Flower, D. R. & Doytchinova, I. A. AllerTOP v.2- a server for in silico prediction of allergens. *J Mol. Model*. **20**, 2278 (2013).

Dimitrov, I., Naneva, L., Doytchinova, I. A. & Bangov, I. AllergenFP: allergenicity prediction by descriptor fingerprints. *Bioinform.* **30**, 846–851 (2014).

Fiers, M. W. E. J., Kleter, G. A., Nijland, H., Peijnenburg, A., Nap, J. P. & Ham, R. Allermatch™, a webtool for the prediction of potential allergenicity according to current FAO/WHO Codex alimentarius guidelines. *BMC Bioinform*. **5**, 133 (2004).

Goodman, R. E., Ebisawa, M., Ferreira, F., Sampson, H. A., van Ree, R., Vieths, S., Baumert, J.L., Bohle, B., Lalithambika, S., Wise, J. and Taylor, S.L. Allergen Online: a peer‐reviewed, curated allergen database to assess novel food proteins for potential cross‐reactivity. *Mol. Nut. & food res.* **60**, 1183-1198 (2016).

Gupta, S., Kapoor, P., Chaudhary, K., Gautam, A. & Kumar, R. Open source drug discovery consortium, Raghava GP in silico approach for predicting toxicity of peptides and proteins. *PLoS One* **8**, 73957 (2013).

Sanner, M. F. Python: a programming language for software integration and development. *J. Mol. Graph Model* **17**, 57–61 (1999).

Morris, G. M., Huey, R., Lindstrom, W., Sanner, M. F., Belew, R. K. & Goodsell, D. S. AutoDock4 and AutoDockTools4: automated docking with selective receptor flexibility. *J. Comput. Chem*. **30**, 2785–2791 (2009).

Kolaskar, A. & Tongaonkar, P. C. A semi-empirical method for prediction of antigenic determinants on protein antigens. *FEBS Lett*. **276**, 172–174 (1990).

Karplus, P. & Schulz, G. Prediction of chain flexibility in proteins. *Natur wissen schaften* **72**, 212–213 (1985).

Jespersen, M. C., Peters, B., Nielsen, M. & Marcatili, P. BepiPred-2.0: improving sequence-based B-cell epitope prediction using conformational epitopes. *Nucleic Acids Res.* **45**, W24–W29 (2017).

Emini, E. A., Hughes, J. V., Perlow, D. & Boger, J. Induction of hepatitis A virus neutralizing antibody by a virus-specific synthetic peptide. *J. Virol.* **55**, 836–839 (1985).

Parker, J., Guo, D. & Hodges, R. New hydrophilicity scale derived from high-performance liquid chromatography peptide retention data: correlation of predicted surface residues with antigenicity and X-ray-derived accessible sites. *Biochem* **25**, 5425–5432 (1986).

Chou, P. & Fasman, G. Prediction of the secondary structure of proteins from their amino acid sequence. *Adv. Enzymol*. **47**, 45–148 (1978).

Rana, A. & Akhter, Y. A multi-subunit based, thermodynamically stable model vaccine using combined immunoinformatics and protein structure based approach. *Immunobiol.* **221**, 544–557 (2016).

Saha, S. & Raghava, G. P. AlgPred: prediction of allergenic proteins and mapping of IgE epitopes. *Nucl. Acids Res*. **34**, W202-9 (2006).

Doytchinova, I. A. & Flower, D. R. VaxiJen: a server for prediction of protective antigens, tumour antigens and subunit vaccines. *BMC Bioinform*. **8**, 4 (2007b).

Hebditch, M., Carballo-Amador, M. A., Charonis, S., Curtis, R. & Warwicker, J. Protein–Sol: a web tool for predicting protein solubility from sequence. *Bioinform.* **33**, 3098–3100 (2017).

Gasteiger, E., Hoogland, C., GattikerA, Duvaud S., Wilkins, M. R., Appel, R. D. & Bairoch, A. Protein identification and analysis tools on the ExPASy server. *Nucleic Acids Res.* **31**, 3784–3788 (2003).

Hasan, M., Joy, Z. F., Bhuiyan, E. H. & Islam, M. S. In Silico characterization and motif election of neurotoxins from Snake venom. *Am. J. Biochem. Biotechnol.* **11**, 84 (2015a).

Kosciolek, T. & Jones, D. T. De novo structure prediction of globular proteins aided by sequence variation-derived contacts. *PLoS One*, **9**, 92197 (2014).

Thaysen-Andersen, M. & Packer, N. H. Site-specific glycoproteomics confirms that protein structure dictates formation of N-glycan type, core fucosylation and branching. *Glycobiol.* **22**, 1440–1452 (2012).

Xu, D. & Zhang, Y. Improving the physical realism and structural accuracy of protein models by a two-step atomic-level energy minimization. *Biophys.* J. **101**, 2525–2534 (2011).

Chen, V. B., Arendall, W. B., Headd, J. J., Keedy, D. A., Immormino, R. M., Kapral, G. J., Murray, L. W., Richardson, J. S. & Richardson, D. C. MolProbity: all-atom structure validation for macromolecular crystallography. *Acta Crystallographica Section D: Biological Crystallography*, **66**, 12-21 (2010).

Craig, D.B. & Dombkowski, A.A. Disulfide by Design 2.0: a web-based tool for disulfide engineering in proteins. *BMC Bioinformatics*. **14**:346 (2013).

Yang, J., Yan, R., Roy, A., Xu, D., Poisson, J. & Zhang, Y. The I-TASSER Suite: protein structure and function prediction. *Nature methods*, **12**, p.7 (2015).

Comeau, S. R., Gatchell, D. W., Vajda, S. & Camacho, C. J. ClusPro: a fully automated algorithm for protein-protein docking. *Nucl. Acids Res.* **32**, W96–W99 (2004).

Macalino, S., Basith, S., Clavio, N., Chang, H., Kang, S. & Choi, S. Evolution of In Silico strategies for protein-protein interaction drug discovery. *Molecules* **23**, 1963 (2018).

Schneidman-Duhovny, D., Inbar, Y., Nussinov, R. & Wolfson, H. J. PatchDock and SymmDock: servers for rigid and symmetric docking. *Nucl. Acids Res.* **33**, W363–W367 (2005).

Mashiach, E., Schneidman-Duhovny, D., Andrusier, N., Nussinov, R. & Wolfson, H.J. FireDock: a web server for fast interaction refinement in molecular docking. *Nucleic Acids Res.* **36**, W229–W232 (2008).

Lopez-Blanco, J. R., Aliaga, J. I., Quintana-Orti, E. S. & Chacon, P. iMODS: internal coordinates normal mode analysis server. *Nucleic Acids Res.* **42**, W271–W276 (2014).

Aalten, D. M. F., Groot, B. L., Findlay, J. B. C., Berendsen, H. J. C. & Amadei, A. A comparison of techniques for calculating protein essential dynamics. *J. Comput. Chem.* **18**, 169–181 (1997).

Wuthrich, K., Wagner, G., Richarz, R. & Braun, W. Correlations between internal mobility and stability of globular proteins. *Biophys.* J. **32**, 549–560 (1980).

Cui, Q. & Bahar, I. Normal mode analysis theoretical and applications to biological and chemical systems. *Briefing Bioinform.* **8**, 378–379 (2007).

Prabhakar, P. K., Srivastava, A., Rao, K. K. & Balaji, P. V. Monomerization alters the dynamics of the lid region in C*ampylobacter jejuni* CstII: an MD simulation study. *J. Biomol. Struct. Dyn.* **34**, 778–779 (2016).

Grote, A. JCat: a novel tool to adapt codon usage of a target gene to its potential expression host. *Nucleic Acids Res*. **33**, W526–W531 (2005).

Solanki, V. & Tiwari, V. Subtractive proteomics to identify novel drug targets and reverse vaccinology for the development of chimeric vaccine against *Acinetobacter baumannii*. *Sci. Rep*. **8**, 9044 (2018).

Velazquez-Roman, J., León-Sicairos, N., deJesusHernández-Díaz, L. & Canizalez-Roman, A. Pandemic *Vibrio parahaemolyticus* O3:K6 on the American continent. *Front. Cell Infect. Microbiol.* **3**, 110 (2014).

Golkar, Z., Bagasra, O. & D. G. Pace, Bacteriophage therapy: a potential solution for the antibiotic resistance crisis. *J. Infect. Dev. Countries* **8**, 129-136 (2014).

Judson, N. & Mekalanos J. J. TnAraOut, a transposon-based approach to identify and characterize essential bacterial genes. *Nature Biotech.* **18**, 740 (2000).

Hossain, M., Chowdhury, D. U. S., Farhana, J., Akbar, M. T., Chakraborty, A., Islam, S., & Mannan, A. Identification of potential targets in Staphylococcus aureus N315 using computer aided protein data analysis. *Bioinformation* **9**, 187 (2013).

Zhang, R., Ou, H. Y. & Zhang, C. T. DEG: a database of essential genes. *Nucleic Acids Res.* **32**, D271-D272 (2004).

Mondal, S.I. Identification of potential drug targets by subtractive genome analysis of Escherichia coli O157: H7: an in silico approach. *Adv. Appl. Bioinform. Chem.* **8**, 49 (2015).

Michael, C. A., Dominey-Howes, D. & Labbate, M. The antimicrobial resistance crisis: causes, consequences, and management. *Front. Public Health* **2**, 145 (2014).

Baliga, P., Shekar, M. & Venugopal M. N. Potential Outer Membrane Protein Candidates for Vaccine Development Against the Pathogen *Vibrio anguillarum*: A Reverse Vaccinology Based Identification. *Curr. Microbiol.* **75**, 368-77 (2018).

Hasan, M., Ghosh, P., Azim, K., Mukta, S., Abir, R. A., Nahar, J. & Khan, M. M. Reverse vaccinology approach to design a novel multi-epitope subunit vaccine against avian influenza A (H7N9) virus. *Microb. Pathog.* **130**, 19-37 (2019a).

Hasan, M., Islam M. S., Chakraborty, S., Mustafa, A. H., Azim, K. F., Joy, Z. F., Hossain, M. N., Foysal, S. H. & Hasan, M. N. Contriving a chimeric polyvalent vaccine to prevent infections caused by herpes simplex virus (type-1 and type-2): an exploratory immunoinformatic approach. J. Biomol. Struct. Dyn. **12,** 1-18 (2019b).

Ghaffari-Nazari, H., Tavakkol-Afshari, J., Jaafari, M. R., Tahaghoghi-Hajghorbani, S., Masoumi, E. & Jalali, S. A. Improving Multi-Epitope Long Peptide Vaccine Potency by Using a Strategy that Enhances CD4+T Help in BALB/c Mice. *PloS one* **10**, e0142563 (2015).

Yang, Y., Sun, W., Guo, J., Zhao, G., Sun, S., Yu, H., Guo, Y., Li, J., Jin, X., Du, L. & Jiang, S. In silico design of a DNA-based HIV-1 multi-epitope vaccine for Chinese populations. *Human Vaccines Immunother.* **11**, 795–805 (2015).

Hasan, M., Azim, K. F., Begum, A., Khan, N. A., Shammi, T. S., Imran, M. A. S., Chowdhury, I. M., Urme, S. R. Vaccinomics strategy for developing a unique multi-epitope monovalent vaccine against Marburg marburgvirus. *Infect. Gene. Evol.* **70**, 140-157 (2019c).

Gulati, A., Kumar, R. & Mukhopadhaya, A. Differential Recognition of *Vibrio parahaemolyticus* OmpU by Toll-Like Receptors in Monocytes and Macrophages for the Induction of Proinflammatory Responses. *Infect. Immun.* **87**, 809-18 (2019).

Figures

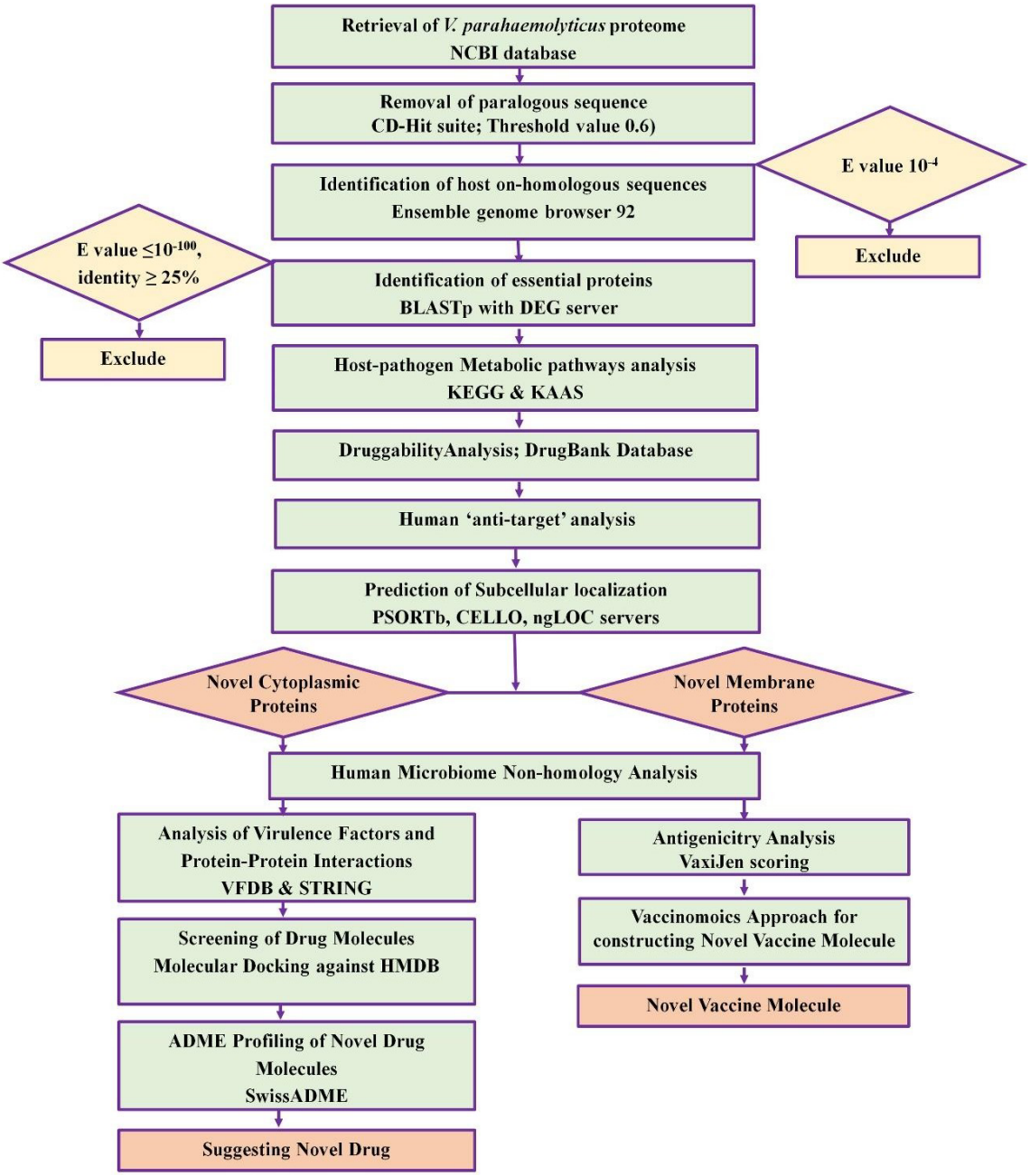

Figure 1. Proteome exploration of *Vibrio parahaemolyticus* to identify novel drug targets.

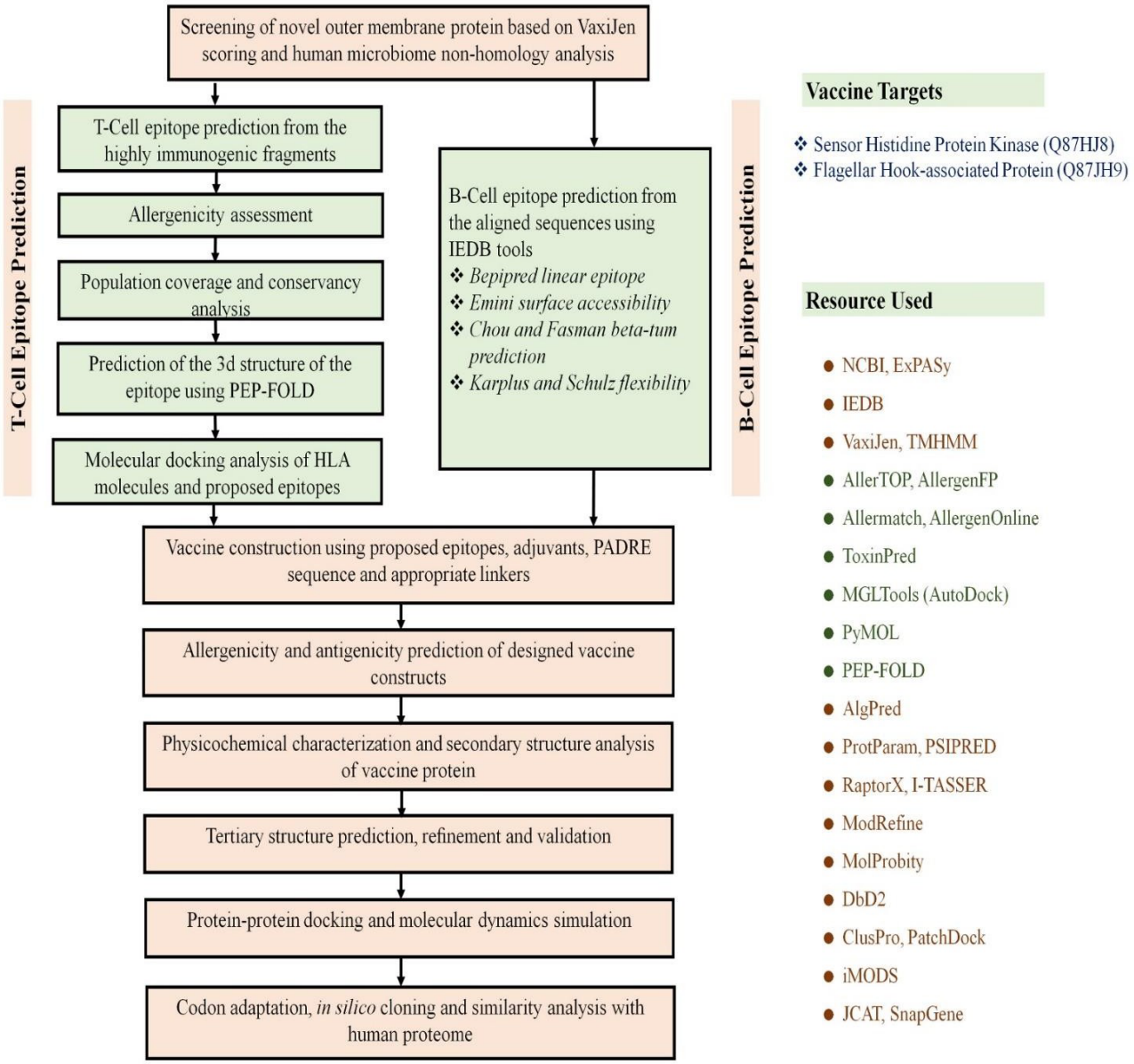

Figure 2. Flow chart summarizing the protocols over multi-epitope subunit vaccine development against *V. parahaemolyticus* through reverse vaccinology approach.

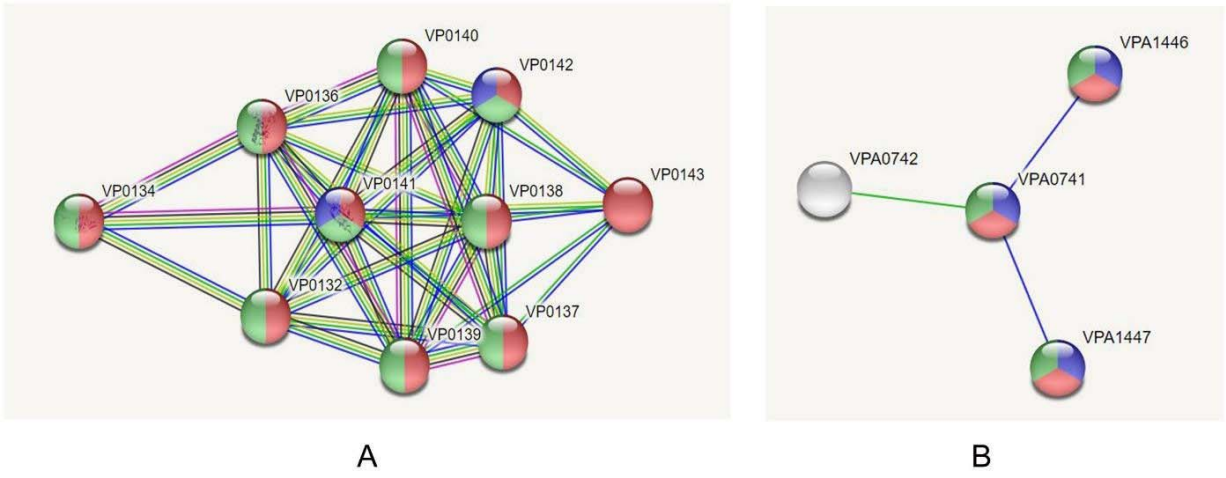

Figure 3. Investigation of Protein-Protein Interactions through STRING v10.5 server; (A) UDP-N-acetylmuramoyl-L-alanyl-D-glutamate--2,6-diaminopimelate ligase (murE), (B) Trigger factor (tig)

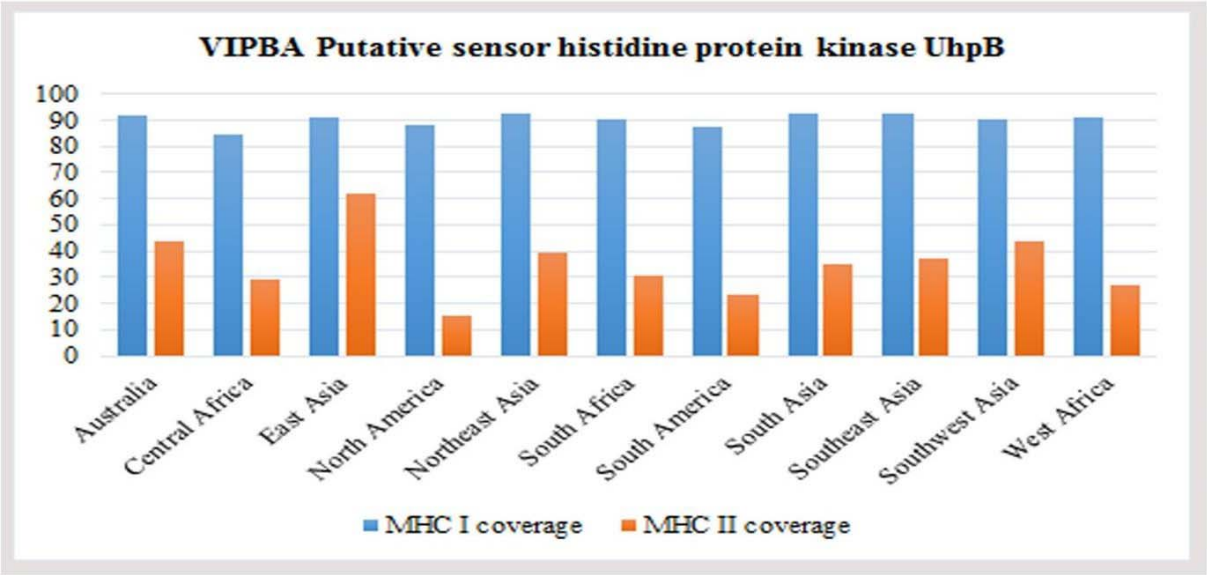

A

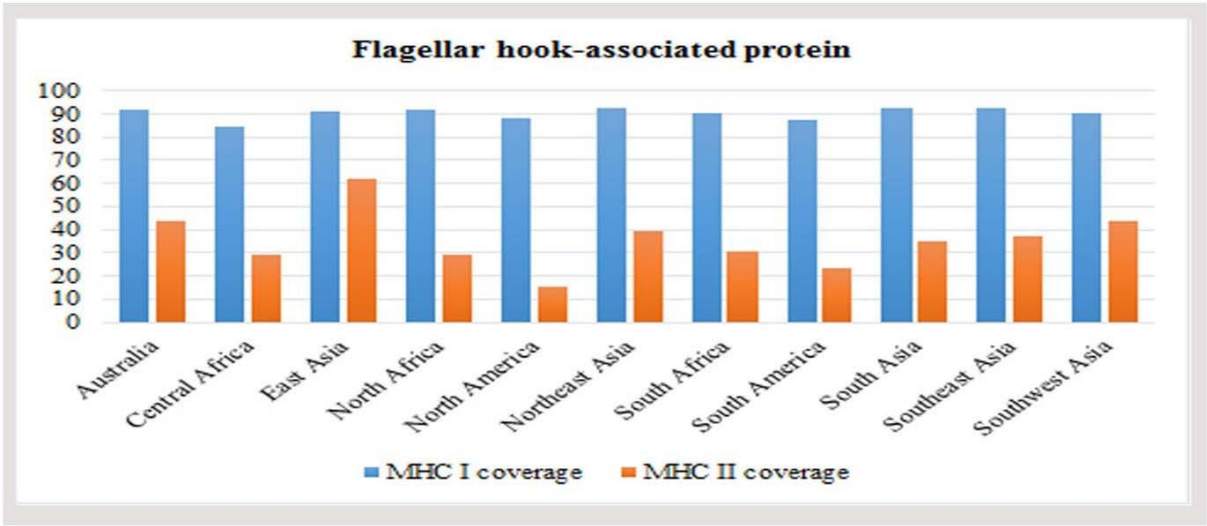

B

Figure 4. Population coverage analysis of (A) VIPBA putative sensor histidine protein kinase UhpB, and (B) Flagellar hook-associated protein.

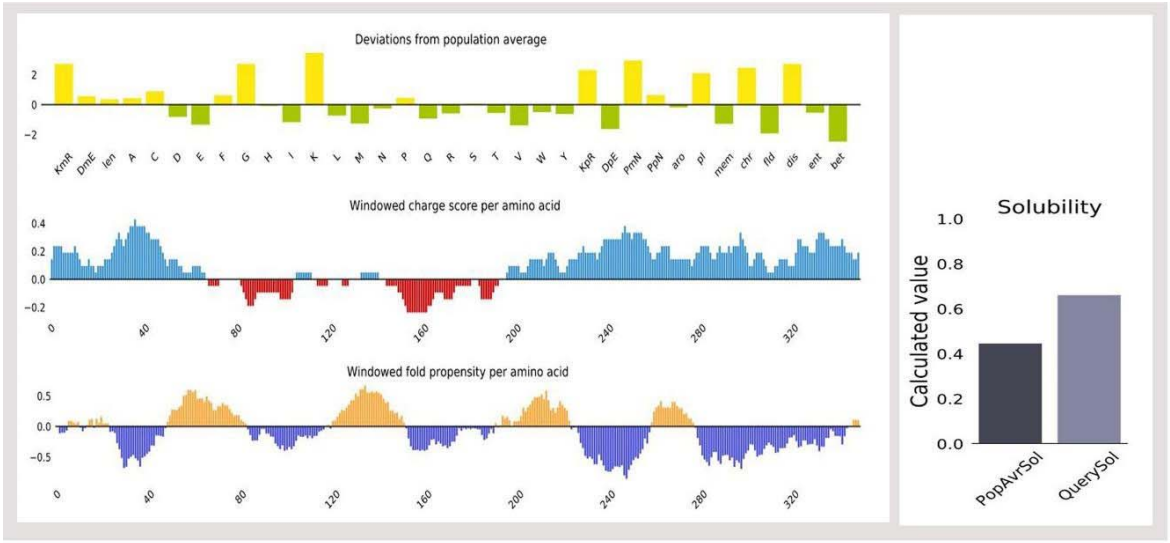

A

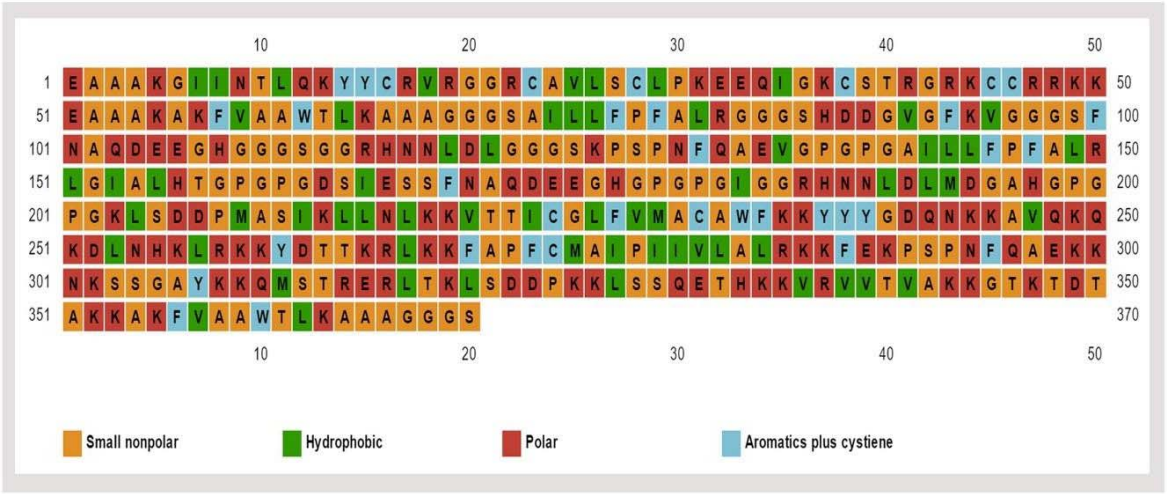

B

Figure 5. Solubility prediction of vaccine constructs. (A) Solubility prediction of designed vaccine construct V1 using via Protein-sol server, and (B) prediction of polar, nonpolar, hydrophobic and aromatic regions.

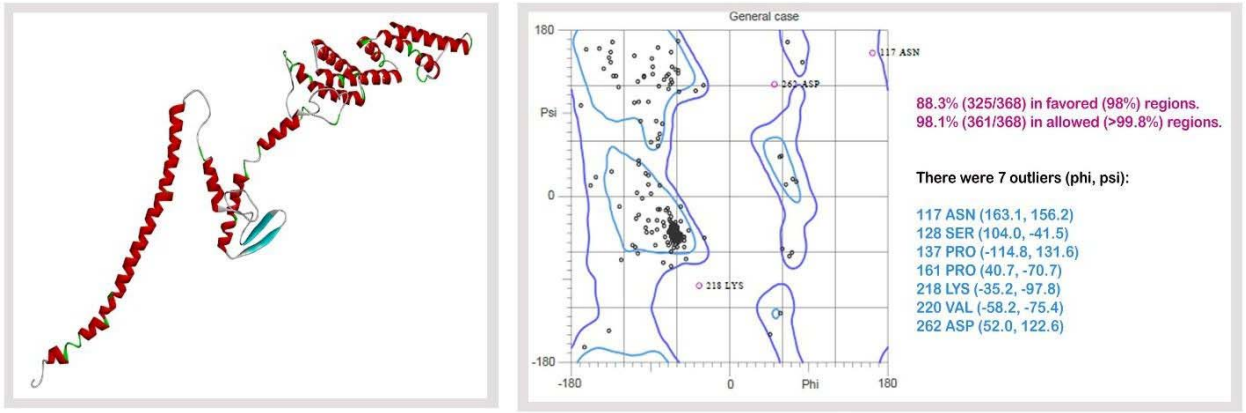

Figure 6. Tertiary structure prediction and validation of vaccine protein V1. (A) Tertiary structure of modeled construct V1, (B) Ramachandran plot analysis of vaccine protein V1.

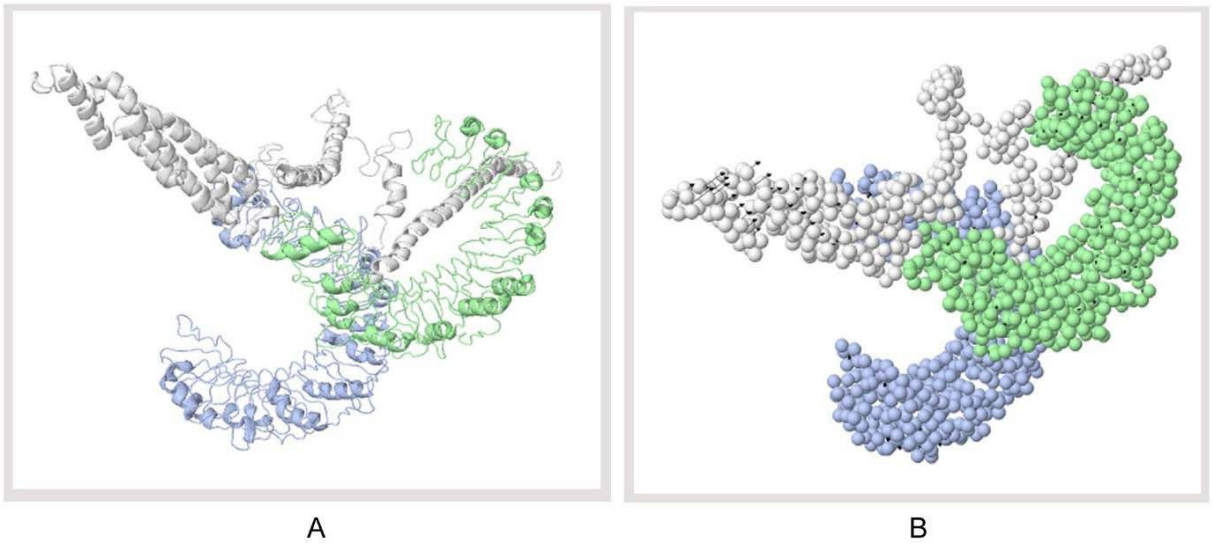

Figure 7. Docked complex of vaccine construct V1 with human TLR 1/2 heterodimer. (A) Cartoon format, and (B) Ball structure.

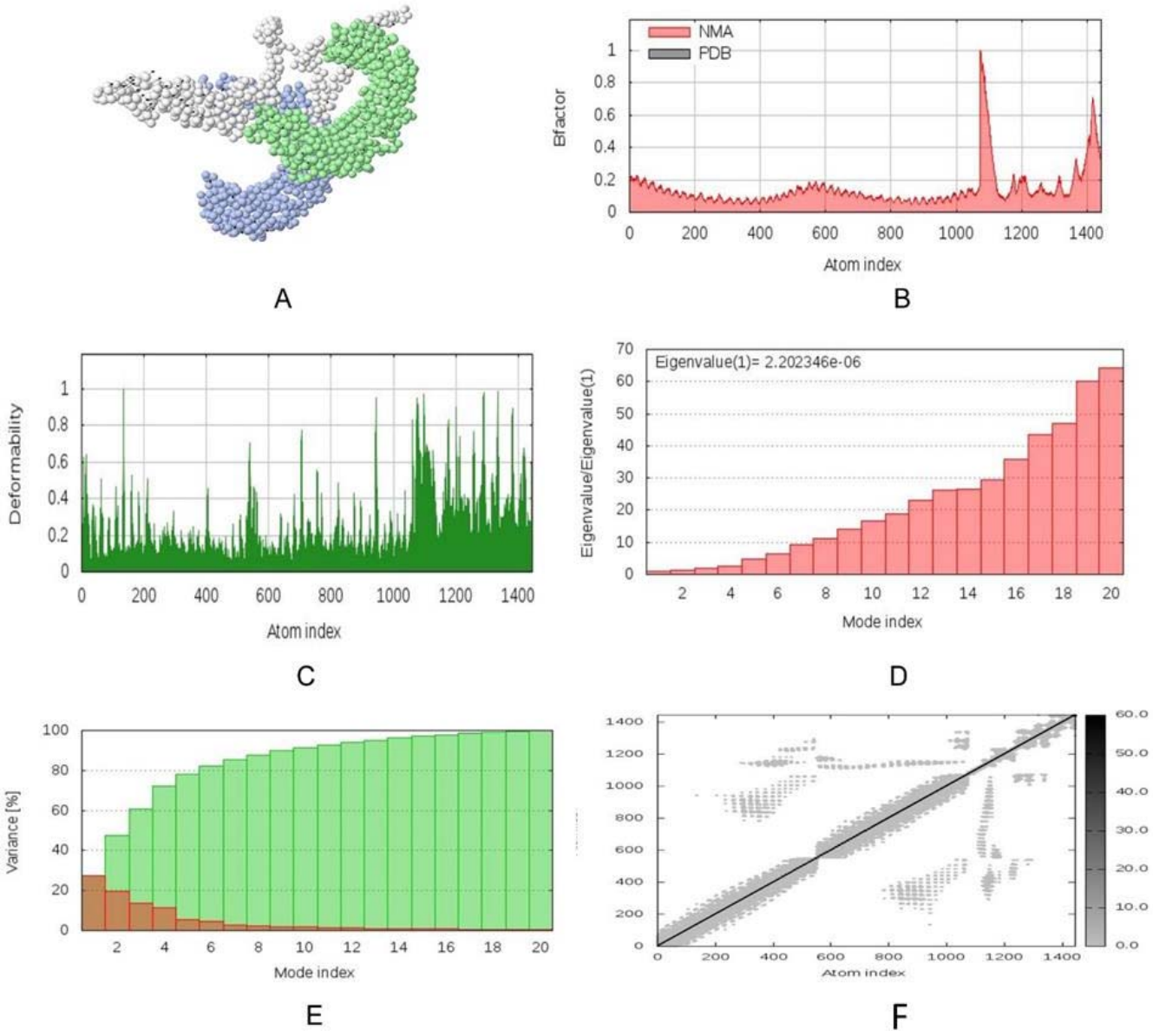

Figure 8. Molecular dynamics simulation of vaccine protein V1-TLR8 complex. Stability of the protein-protein complex was investigated through (A) mobility, (B) B-factor, (C) deformability, (D) eigenvalue, (E) covariance and (F) elastic network analysis.

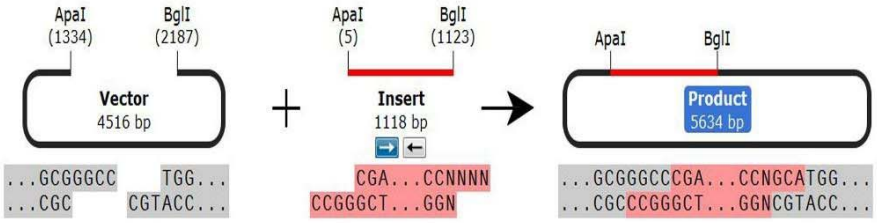

A

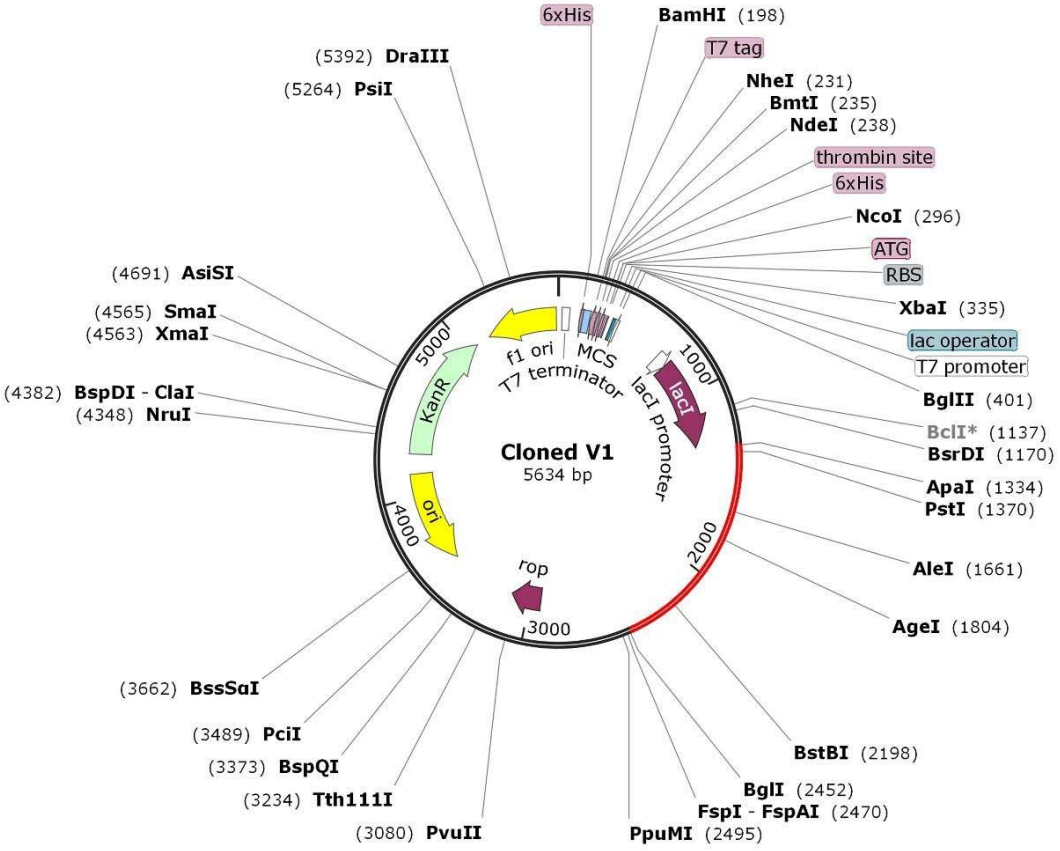

B

Figure 9. In silico restriction cloning of the gene sequence of construct V1 into pET28 a(+) expression vector; (A) Codon adaptation (B) Restriction digestion of the vector pET28 a(+) and construct V1 with BglI and ApaI (C) Inserted desired fragment (V1 Construct) between ApaI (1334) and BglI (2452) indicated in red color.

Supplementary Figures

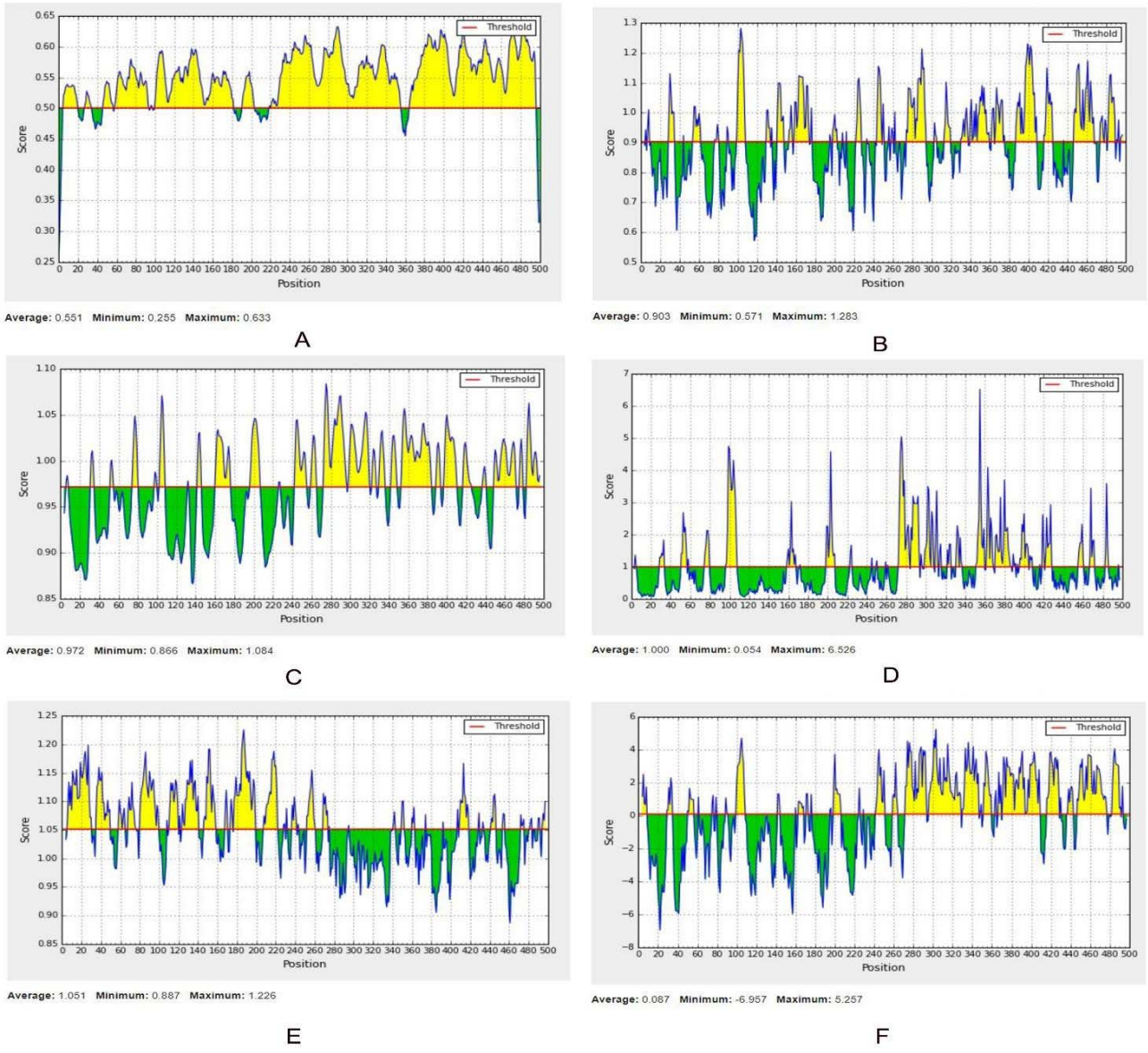

Supplementary Figure 1. B-cell epitope prediction of Sensor histidine protein kinase UhpB (A: Linear, B: Beta-turn, C: Flexibility, D: Surface Accessibility, E: Antigenicity, F: Hydrophilicity). For each graph, X-axis and Y-axis represent the position and score. Residues that fall above the threshold value are shown in yellow color while the highest peak in yellow color identifies most favored position.

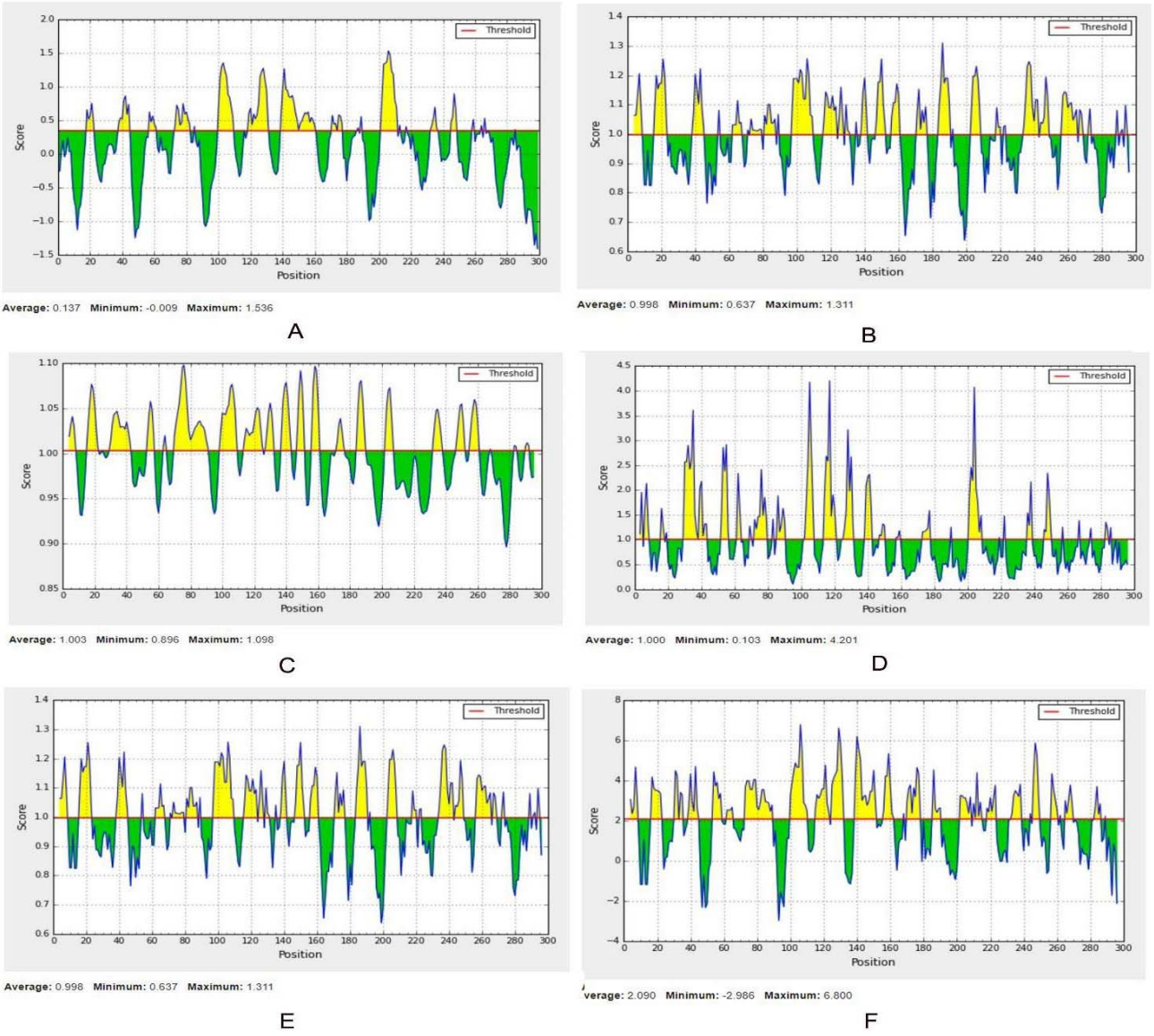

Supplementary Figure 2. B-cell epitope prediction of Flagellar hook-associated protein (A: Linear, B: Beta-turn, C: Flexibility, D: Surface Accessibility, E: Antigenicity, F: Hydrophilicity). For each graph, X-axis and Y-axis represent the position and score. Residues that fall above the threshold value are shown in yellow color while the highest peak in yellow color identifies most favored position.

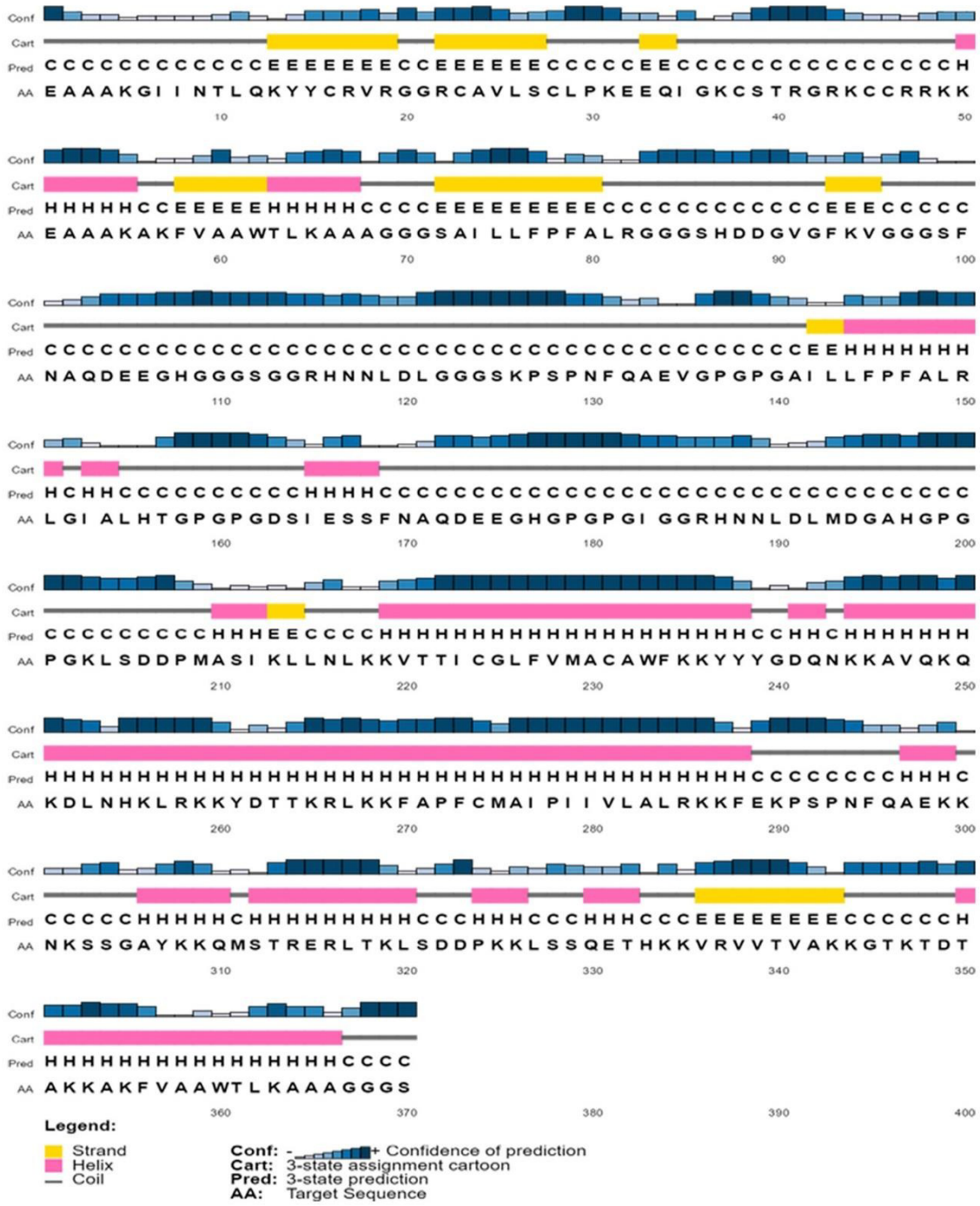

Supplementary Figure 3. Secondary structure prediction of constructed vaccine protein V1 using PESIPRED server.

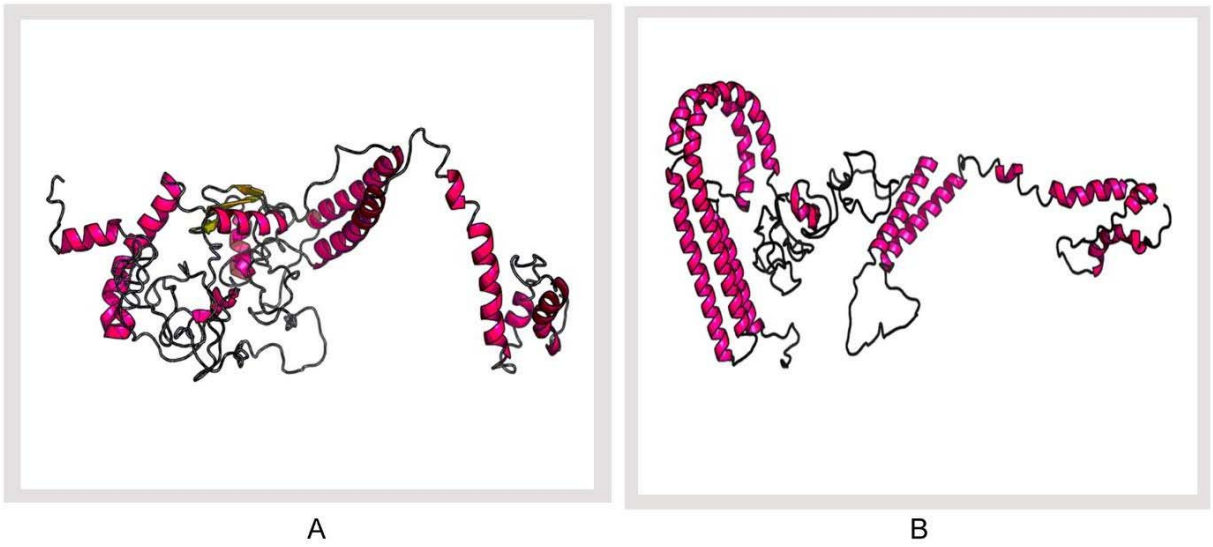

Supplementary Figure 4. 3D modeled structure of vaccine protein. (A) V2 and (B) V3 generated via RaptorX server.

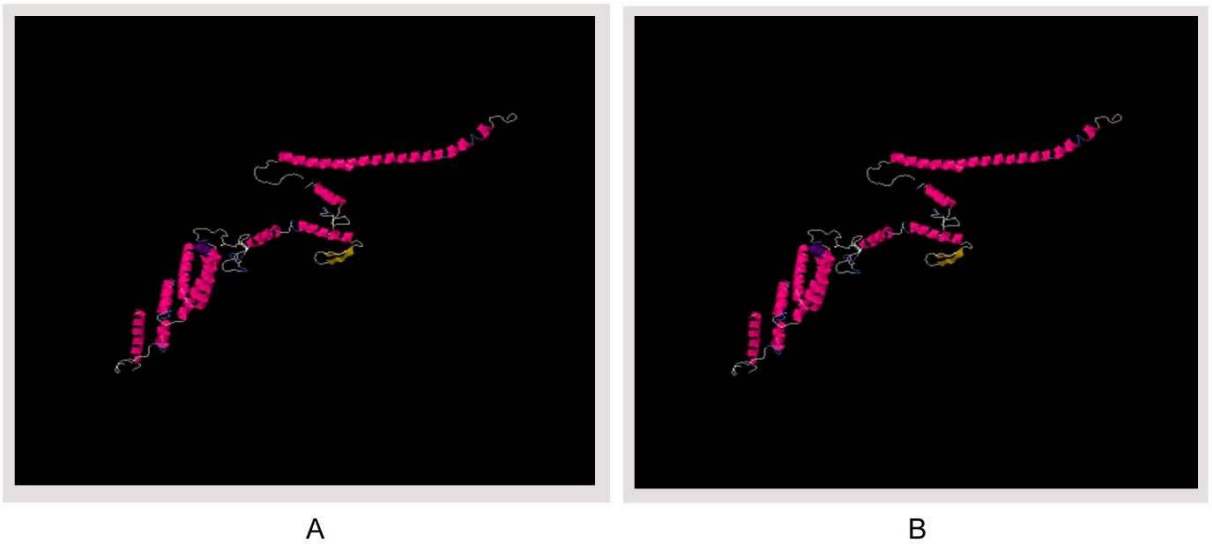

Supplementary Figure 5. Disulfide engineering of vaccine protein V1. (A) Initial form, (B) Mutant form.

Tables

Table 1: Subtractive genomic analysis scheme

Sl. No.	Steps	No. of proteins	Protein sets
1.	Total number of proteins	4822	Set 0 (Supplementary file 1)
2.	Non-paralogous (>60% identical) in CD-Hit	4729	Set 1 (Supplementary file 2)
3.	proteins with >100 amino acids	4123	Set 2 (Supplementary file 3)
4.	Number of proteins nonhomologous to *H. sapiens* using BLASTp (E value 10^{-3})	3164	Set 3 (Supplementary file 4)
5.	Essential proteins in DEG 15.2 server (E value $\leq 10^{-100}$, Bit score >100)	1107	Set 4 (Supplementary file 5)
6.	Essential Proteins involved only in unique metabolic pathways (KAAS at KEGG)	96	Set 5 (Supplementary file 9)
7.	Essential proteins found to be novel in Drug Bank 5.1.0 (using default parameters)	41	Set 6 (Supplementary file 10)
8.	Novel drug target proteins non-homologous to 'anti-targets' using BLASTp (E value <0.005, Identity <25%, Query length >30%)	41	Set 7 (Supplementary file 10)
9.	Essential cytoplasmic proteins using PSORTb, CELLO, ngLOC, PSLpred	16	Set 8 (Supplementary file 12)
10.	Proteins showing <45% similarity with human microflora proteins	9	Set 9 (Supplementary file 13)
11.	Identified virulence associated novel proteins by VFDB analysis	2	Set 10 (Table 4)
12.	Essential membrane proteins using PSORTb, CELLO, ngLOC, PSLpred	25	Set 11 (Supplementary file 14)
13.	Identified vaccine targets with less similarity with human microflora proteins and antigenicity	2	Set 12 (Table 7)

Table 2: Pathogen specific essential cytoplasmic proteins as novel therapeutic targets.

Sl. No	Protein Id	KO assignment	Description	Pathways
1.	Q87L83	K09823	Fur family transcriptional regulator, zinc uptake regulator	Quorum sensing
2.	Q87GW9	K07674	Two-component system, narl family, nitrate/nitrite sensor histidine kinase narq	Two-component system
3.	Q79YW1	K02410	Flagellar motor switch protein flig	Bacterial chemotaxis
4.	Q87HD9	K11904	Type VI secretion system secreted protein vgrg	Bacterial secretion system
5.	Q87TC9	K02461	General secretion pathway protein L	Bacterial secretion system
6.	Q87NV3	K07780	Arac family transcriptional regulator required for anaerobic and stationary phase induction of genes	Two-component system
7.	Q87K78	K07718	Two-component system, sensor histidine kinase yesm	Two-component system
8.	Q87I65	K07688	Two-component system, narl family, response regulator, fimbrial Z protein, fimz	Two-component system
9.	Q87TD5	K02455	General secretion pathway protein F	Biofilm formation
10.	Q87MI1	K03567	Glycine cleavage system transcriptional repressor	Biofilm formation
11.	Q87HC5	K11892	Type VI secretion system protein impk	Bacterial secretion system
12.	Q87Q12	K02053	Putative spermidine/putrescine transport system permease protein	Quorum sensing
13.	Q87LE2	K03092	RNA polymerase sigma-54 factor	Biofilm formation
14.	Q87HC6	K11891	Type VI secretion system protein impl	Biofilm formation
15.	Q79YX4	K03408	Purine-binding chemotaxis protein chew	Bacterial chemotaxis
16.	Q87NG0	K11617	Two-component system, narl family, sensor histidine kinase lias	Two-component system

Table 3: Predicted therapeutic targets (novel cytoplasmic proteins) showing virulent properties.

Novel drug targets	Accession Id	VFDB analysis	Interacted proteins
VIBPA Type II secretion system protein L	Q87TC9	5 hits	9
VIBPA Putative fimbrial protein Z	Q87I65	4 hits	3

Table 4: Top 10 metabolites predicted as suitable drug candidates against VIBPA Type II secretion system protein L and VIBPA Putative fimbrial protein Z.

Novel Targets	HMDB ID	Binding Energy	Name	Drug Bank ID	Drug Name	Drug Group	
VIBPA Type II secretion system protein L (Q87TC9)	HMDB0004971	-10.6	Glucosylceramide (d18:1/16:0)	DB09039	Eliglustat	Approved	
	HMDB0004972	-10.5	Glucosylceramide (d18:1/18:0)	DB09039	Eliglustat	Approved	
	HMDB0004970	-10.3	Glucosylceramide (d18:1/9Z-18:1)	DB09039	Eliglustat	Approved	
	HMDB0004976	-10.3	Glucosylceramide (d18:1/26:1(17Z))	DB09039	Eliglustat	Approved	
	HMDB0008646	-10.3	PC(22:4(7Z,10Z,13Z,16Z)/22:4(7Z,10Z,13Z,16Z))	DB00641	Simvastatin	Approved	
	HMDB0011300	-10.1	PC(P-18:1(11Z)/P-18:1(11Z)	DB00334	Olanzipine	Approved, Investigational	
	HMDB0008443	-9.7	PC(20:4(5Z,8Z,11Z,14Z)/20:4(5Z,8Z,11Z,14Z))	DB00641	Simvastatin	Approved	
	HMDB0008138	-9.6	PC(18:2(9Z,12Z)/18:2(9Z,12Z))	DB00641	Simvastatin	Approved	
	HMDB0004973	-9.5	Glucosylceramide (d18:1/20:0)	DB09039	Eliglustat	Approved	
	HMDB0010348	-9.5	Dehydroepiandrosterone 3-glucuronide	DB01708	Prasterone	Approved, Investigationa, Nutraceutical	
VIBPA Putative fimbrial protein Z (Q87I65)	HMDB0004972	-9.6	Glucosylceramide (d18:1/18:0)	DB09039	Eliglustat	Approved	
	HMDB0002308	-9.5	Hydroxocobalamin	DB00200	Hydroxocobalamin	Approved	
	HMDB0004970	-9.3	Glucosylceramide (d18:1/9Z-18:1)	DB09039	Eliglustat	Approved	
	HMDB0004971	-9.3	Glucosylceramide (d18:1/16:0)	DB09039	Eliglustat	Approved	
	HMDB0002174	-9.1	Cobalamin	DB14098	Cobalamin	Experimental	
	HMDB0008646	-8.9	PC(22:4(7Z,10Z,13Z,16Z)/22:4(7Z,10Z,13Z,16Z))	DB00641	Simvastatin	Approved	
	HMDB0060546	-8.9	Norbuprenorphine	DB01026	Ketoconazole	Approved, Investigational	
	HMDB0041936	-8.7	Morphine-3-glucuronide	DB00295	Morphine	Approved, Investigational	
	HMDB0004974	-8.6	Glucosylceramide (d18:1/22:0)	DB09039	Eliglustat	Approved	
	HMDB0008443	-8.5	PC(20:4(5Z,8Z,11Z,14Z)/20:4(5Z,8Z,11Z,14Z))	DB00641	Simvastatin	Approved	

Table 5: ADME profiling of top drug candidates.

ADME analysis		Top drug candidates		
		Eliglustat	***Simvastatin***	***Hydroxocobalamin***
Physicochemical parameters	Formula	C23H36N2O4	C25H38O5	C62H89CoN13O15P
	Molecular weight	404.54 g/mol	418.57 g/mol	1346.36 g/mol
	Molar Refractivity	120.69	118.47	352.74
	TPSA	74.52 Å²	72.83 Å²	468.89 Å²
Lipophilicity	Log $P_{o/w}$ (iLOGP)	4.07	3.74	0.00
	Log $P_{o/w}$ (XLOGP3)	4.02	4.68	-3.48
	Log $P_{o/w}$ (WLOGP)	3.57	4.59	-0.99
	Log $P_{o/w}$ (MLOGP)	2.27	3.77	-3.84
	Log $P_{o/w}$ (SILICOS-IT)	4.88	3.77	-4.08
	Consensus Log $P_{o/w}$	3.76	4.11	-2.48
	Log $P_{o/w}$ (iLOGP)	4.07	3.74	0.00
Pharmacokinetics	GI absorption	High	High	Low
	BBB permeant	Yes	No	No
	P-gp substrate	No	No	Yes
	CYP1A2 inhibitor	No	No	No
	CYP2C19 inhibitor	No	No	No
	CYP2C9 inhibitor	No	Yes	No
	CYP2D6 inhibitor	Yes	No	No
	CYP3A4 inhibitor	No	Yes	No
	Log K_p (skin permeation)	-5.91 cm/s	-5.53 cm/s	-16.98 cm/s
Water Solubility	Log *S* (SILICOS-IT)	-5.05	-3.56	-7.11
	Solubility	3.57e-03 mg/ml ; 8.83e-06 mol/l	1.15e-01 mg/ml ; 2.74e-04 mol/l	1.04e-04 mg/ml ; 7.73e-08 mol/l
	Class	Moderately soluble	Soluble	Poorly soluble
Druglikeness	Bioavailability Score	0.55	0.55	0.17
	Lipinski	Yes; 0 violation	Yes; 0 violation	No; 3 violations: MW>500, NorO>10, NHorOH>5
	Ghose	Yes	Yes	No; 4 violations: MW>480, WLOGP<-0.4, MR>130,
	Veber	No; 1 violation: Rotors>10	Yes	No; 2 violations: Rotors>10, TPSA>140
Medicinal Chemistry	Synthetic accessibility	4.76	5.80	10.00
	PAINS	0 alert	0 alert	0 alert
	Brenk	2 alerts: imine_1, imine_2	1 alert: more_than_2_esters	1 alert: phosphor
	Leadlikeness	No; 3 violations: MW>350, Rotors>7, XLOGP3>3.5	No; 2 violations: MW>350, XLOGP3>3.5	No; 2 violations: MW>350, Rotors>7

Table 6: Novel vaccine targets proteins showing higher antigenicity

Accession No.	Protein name	VaxiJen score	Similarity with human microbiome (%)
Q87HJ8	Sensor histidine protein kinase UhpB	0.65	<45
Q87JH9	Flagellar hook-associated protein	0.53	<41

Table 7: Predicted final CTL and HTL epitopes of histidine protein kinase and flagellar hook-associated protein

Protein	MHC	Epitope	Start	End	Vaxijen	Conservancy
Sensor histidine protein kinase UhpB	MHC-I	AILLFPFAL	36	44	2.993	99.00%
		ILLFPFALR	37	45	2.9721	99.00%
		HDDGVGFKV	448	456	2.363	99.00%
	MHC-II	ILLFPFALRLGIALH	37	51	2.1484	87.00%
		AILLFPFALRLGIAL	36	50	1.9451	87.00%
		LLFPFALRLGIALHT	38	52	1.8268	87.00%
Flagellar hook-associated protein	MHC-I	FNAQDEEGH	125	133	1.8425	98.00%
		GGRHNNLDL	234	242	1.7855	99.00%
		KPSPNFQAEV	203	212	1.4978	45.00%
	MHC-II	DSIESSFNAQDEEGH	199	133	1.304	88.00%
		IGGRHNNLDLMDGAH	233	247	0.801	59.00%
		KLSDDPMASIKLLNL	38	52	0.887	88.00%

Table 8: Binding energy of predicted epitopes with selected MHC class I and MHC class II molecules generated from molecular docking by AutoDock

Protein	Epitope	MHC Class	Binding Energy
Sensor histidine protein kinase	FNAQDEEGH	HLA-A*11:01	-8.6
	GGRHNNLDL		-9.1
	KPSPNFQAEV		-8.2
	DSIESSFNAQDEEGH	HLA-DRB1*04:01	-7.3
	IGGRHNNLDLMDGAH		-6.5
	KLSDDPMASIKLLNL		-6.3
Flagellar hook-associated protein	AILLFPFAL	HLA-A*11:01	-8.3
	ILLFPFALR		-8.1
	HDDGVGFKV		-8.1
	ILLFPFALRLGIALH	HLA-DRB1*04:01	-7.0
	AILLFPFALRLGIAL		-6.4
	LLFPFALRLGIALHT		-7.2

Supplementary Tables

Supplementary Table 1: Pathway dependent metabolic proteins with druggable properties.

Accession Id	Pathway involved	Drug bank id	Drug name	E value
Q87T41	Biosynthesis of antibiotics	DB03161	Thymidine-5'-Diphospho-Beta-D-Xylose	6.48766e-14
		DB03751	2'deoxy-Thymidine-5'-Diphospho-Alpha-D-Glucose	
Q87LD8	Phosphotransferase system	DB01899	Nd1-Phosphonohistidine	6.74952e-08
Q87GN8	Two-component system	DB04395	Phosphoaminophosphonic Acid-Adenylate Ester	1.72082e-18
Q79YV7	Two-component system	DB02671	1-Methylimidazole	2.24743e-12
		DB03366	Imidazole	
Q87R58	Two-component system	DB09462	Glycerin	6.34798e-11
Q87GX4	beta-Lactam resistance	DB09462	Glycerin	4.25465e-42
Q87RK0	Phosphotransferase system	DB08357	1-Ethoxy-2-(2-Ethoxyethoxy)Ethane	3.64017e-78
Q87MK4	Two-component system	DB02524	2',3'-O-{4-[Hydroxy(oxido)-λ5-azanylidene]-2,6-dinitro-2,5-cyclohexadiene-1,1-diyl}adenosine 5'-(tetrahydrogen triphosphate)	1.75895e-105
		DB03909	Adenosine-5'-[Beta, Gamma-Methylene]Triphosphate	
		DB04395	Phosphoaminophosphonic Acid-Adenylate Ester	
Q79YV8	Two-component system	DB01857	Phosphoaspartate	7.12121e-92
Q87I33	Microbial metabolism in diverse environments	DB01676	Trinitrotoluene	3.17226e-103
		DB02060	Cyclohexanone	
		DB03247	Flavin mononucleotide	
		DB03651	Picric acid	
		DB04528	2,4-Dinitrophenol	
		DB07373	Androsta-1,4- Diene-3,17-Dione	
		DB02508	Isopentyl Pyrophosphate	
		DB11090	Potassium nitrate	
Q87GN9	Two-component system	DB09462	Glycerin	3.29994e-07
Q87RQ5	Beta-Lactam resistance	DB01326 DB00923	Cefamandole Ceforanide	3.70867e-68
Q87QE7	Two-component system	DB02355	Adenosine-5'-Rp-Alpha-Thio-Triphosphate	3.22519e-09
		DB02596	Alpha,Beta-Methyleneadenosine-5'-	
		DB07706	Triphosphate 2-Hydroxyestradiol	
Q87FT7	Microbial metabolism in diverse environments	DB03247	Flavin mononucleotide	2.93774e-98
		DB03793	Benzoic Acid	
Q79YX1	Two-component system	DB09462	Glycerin	9.53705e-09
Q87SD5	Two-component system	DB01857	Phosphoaspartate	2.98609e-09
Q87NJ3	Folate biosynthesis	DB01942	Formic Acid	3.87202e-178
Q87H50	Biofilm formation	DB01972	Guanosine-5'-Monophosphate	3.60354e-26
Q87SQ6	Phosphotransferase system	DB08357	1-Ethoxy-2-(2-Ethoxyethoxy)Ethane	5.27414e-78
Q87FY2	Two-component system	DB01857	Phosphoaspartate	2.44477e-78
Q87QT0	Two-component system	DB02355	Adenosine-5'-Rp-Alpha-Thio-Triphosphate	9.6571e-23
		DB02596	Alpha,Beta-Methyleneadenosine-5'-Triphosphate	
		DB07706	2-Hydroxyestradiol	
Q87K89	Two-component system	DB02355	Adenosine-5'-Rp-Alpha-Thio-Triphosphate	7.00351e-35
		DB02596	Alpha,Beta-Methyleneadenosine-5'-Triphosphate	
		DB07706	2-Hydroxyestradiol	
Q87LQ8	Biofilm formation	DB08874	Fidaxomicin	6.79493e-67
Q79YZ2	Bacterial chemotaxis	DB02461	S-Methyl Phosphocysteine 3-Aminosuccinimide	2.39514e-07
		DB03487	Aspartate Beryllium	
		DB04156	Trifluoride	
Q87TF1	Two-component system	DB01857	Phosphoaspartate	0.0
Q87PF5	Two-component system	DB02355	Adenosine-5'-Rp-Alpha-Thio-Triphosphate	8.10461e-33
		DB02596	Alpha,Beta-Methyleneadenosine-5'-Triphosphate	
		DB07706	2-Hydroxyestradiol	
Q87P07	Two-component system	DB01857	Phosphoaspartate	1.93619e-07
Q87TN0	Beta-Lactam resistance	DB09462	Glycerin	9.07529e-20

Q87N38	Two-component system	DB02355	Adenosine-5'-Rp-Alpha-Thio-Triphosphate	8.70626e-06
		DB02596	Alpha,Beta-Methyleneadenosine-5'-Triphosphate	
		DB07706	2-Hydroxyestradiol	
Q87H65	Two-component system	DB04395	Phosphoaminophosphonic Acid-Adenylate Ester	1.61933e-07
Q87L60	Biofilm formation	DB03793	Benzoic Acid	7.34907e-131
Q87KT8	Biofilm formation	DB01972	Guanosine-5'-Monophosphate	3.51963e-28
Q87H96	Biofilm formation	DB01972	Guanosine-5'-Monophosphate	5.15207e-21
Q87G70	Biofilm formation	DB03793	Benzoic Acid	5.53374e-08
Q87P19	Biofilm formation	DB03142	Alpha-L-Arabinose	7.45968e-10
		DB04062	Beta-D-Fucose	
Q87GX0	Two-component system	DB02355	Adenosine-5'-Rp-Alpha-Thio-Triphosphate	5.03724e-06
		DB02596	Alpha,Beta-Methyleneadenosine-5'-Triphosphate	
		DB07706	2-Hydroxyestradiol	
Q87SA3	Phosphotransferase system	DB08357	1-Ethoxy-2-(2-Ethoxyethoxy)Ethane	0.0
Q87LW1	Peptidoglycan biosynthesis	DB01329	Cefoperazone	0.0
		DB00430	Cefpiramide	
		DB00438	Ceftazidime	
		DB09050	Ceftolozane	
Q87LZ0	Peptidoglycan biosynthesis	DB00760	Meropenem	4.1457e-104
		DB01329	Cefoperazone	
		DB01331	Cefoxitin	
		DB01328	Cefonicid	
		DB00303	Ertapenem	
		DB04570	Latamoxef	
		DB00417	Phenoxymethylpenicillin	
Q87TB5	Two-component system	DB04395	Phosphoaminophosphonic Acid-Adenylate Ester	1.89214e-141
Q87R82	Two-component system	DB02671	1-Methylimidazole	3.37532e-25
		DB03366	Imidazole	
Q87TM1	Quorum sensing	DB03374	3,5-Diiodotyrosine	1.06301e-15
Q87SH0	Beta-Lactam resistance	DB01598	Imipenem	2.19002e-36
		DB01329	Cefoperazone	
		DB01327	Cefazolin	
		DB01163	Amdinocillin	
		DB01328	Cefonicid	
		DB01413	Cefepime	
		DB01415	Ceftibuten	
		DB00948	Mezlocillin	
		DB00438	Ceftazidime	
		DB00303	Ertapenem	
		DB06211	Doripenem	
Q87IT0	Beta-Lactam resistance	DB04233	(Hydroxyethyloxy)Tri(Ethyloxy)Octane	1.48083e-11
		DB07084	N-(6,7,9,10,17,18,20,21-octahydrodibenzo[b,k][1,4,7,10,13,16] hexaoxacyclooctadecin-2-yl)acetamide	
		DB13092	Meclocycline	
Q87G68	Two-component system	DB02365	1,10-Phenanthroline	3.05491e-08
Q87HG5	Bacterial chemotaxis	DB02365	1,10-Phenanthroline	7.39316e-13
Q87G84	Two-component system	DB02671	1-Methylimidazole	5.05136e-06
	Two-component system	DB03366	Imidazole	
Q87NX1	Quorum sensing	DB02451	B-nonylglucoside	9.12499e-09
Q87QR1	Bacterial chemotaxis	DB02365	1,10-Phenanthroline	1.83281e-14
Q87KZ7	Bacterial chemotaxis	DB02365	1,10-Phenanthroline	2.0555e-14
Q87G25	Bacterial chemotaxis	DB02365	1,10-Phenanthroline	5.82633e-15
Q87TN1	Beta-Lactam resistance	DB03825	Rhodamine 6G	1.21402e-137
		DB04209	Dequalinium	
		DB03619	Deoxycholic Acid	
Q87IW5	Two-component system	DB02365	1,10-Phenanthroline	3.83631e-13
Q87QG4	Bacterial chemotaxis	DB02365	1,10-Phenanthroline	2.14253e-08
Q87K74	Bacterial chemotaxis	DB02365	1,10-Phenanthroline	7.72671e-13

Supplementary Table 2: Predicted binding energy (docking score) of novel cytoplasmic proteins with human metabolites

Protein	HMDB ID	Energy	Protein	HMDB ID	Energy
VIBPA Type II secretion system protein (Q87TC9)	HMDB0004971	-10.6	*VIBPA Putative fimbrial protein Z (Q87I65)*	HMDB0004972	-9.6
	HMDB0004972	-10.5		HMDB0002308	-9.5
	HMDB0004970	-10.3		HMDB0004970	-9.3
	HMDB0004976	-10.3		HMDB0004971	-9.3
	HMDB0008646	-10.3		HMDB0002174	-9.1
	HMDB0011300	-10.1		HMDB0008646	-8.9
	HMDB0008443	-9.7		HMDB0060546	-8.9
	HMDB0008138	-9.6		HMDB0041936	-8.7
	HMDB0004973	-9.5		HMDB0004974	-8.6
	HMDB0010348	-9.5		HMDB0008443	-8.5
	HMDB0002308	-9.4		HMDB0010348	-8.5
	HMDB0060824	-9.4		HMDB0004973	-8.4
	HMDB0001993	-9.3		HMDB0008376	-8.4
	HMDB0002961	-9.3		HMDB0008138	-8.3
	HMDB0004974	-9.3		HMDB0010321	-8.3
	HMDB0042005	-9.3		HMDB0010339	-8.3
	HMDB0000077	-9.2		HMDB0041917	-8.3
	HMDB0004246	-9.2		HMDB0000063	-8.2
	HMDB0007934	-9.2		HMDB0041937	-8.1
	HMDB0000015	-9.1		HMDB0003033	-8
	HMDB0000234	-9.1		HMDB0004969	-8
	HMDB0008376	-9.1		HMDB0008036	-8
	HMDB0001926	-9		HMDB0008172	-8
	HMDB0004969	-9		HMDB0060947	-8
	HMDB0000063	-8.9		HMDB0000015	-7.9
	HMDB0000374	-8.9		HMDB0000374	-7.9
	HMDB0000626	-8.9		HMDB0000626	-7.9
	HMDB0010339	-8.9		HMDB0004976	-7.9
	HMDB0041936	-8.9		HMDB0011300	-7.9
	HMDB0004975	-8.8		HMDB0004975	-7.8
	HMDB0011334	-8.8		HMDB0008070	-7.8
	HMDB0000253	-8.7		HMDB0012458	-7.8
	HMDB0001032	-8.7		HMDB0000518	-7.7
	HMDB0002103	-8.7		HMDB0001375	-7.7
	HMDB0004979	-8.7		HMDB0011334	-7.7
	HMDB0008172	-8.7		HMDB0000016	-7.6
	HMDB0014440	-8.7		HMDB0000637	-7.6
	HMDB0000016	-8.6		HMDB0002103	-7.6

	HMDB0000518	-8.6		HMDB0000067	-7.5
	HMDB0000637	-8.6		HMDB0009637	-7.5
	HMDB0002174	-8.6		HMDB0000037	-7.4
	HMDB0008070	-8.6		HMDB0000053	-7.4
	HMDB0060546	-8.6		HMDB0000077	-7.4
	HMDB0001170	-8.5		HMDB0001032	-7.4
	HMDB0008036	-8.5		HMDB0001926	-7.4
	HMDB0010321	-8.5		HMDB0001993	-7.4
	HMDB0041937	-8.5		HMDB0002961	-7.4
	HMDB0003550	-8.4		HMDB0014440	-7.4
	HMDB0000561	-8.3		HMDB0042005	-7.4
	HMDB0003033	-8.3		HMDB0000153	-7.3
	HMDB0004977	-8.3		HMDB0000234	-7.3
	HMDB0006736	-8.3		HMDB0000253	-7.3
	HMDB0009637	-8.3		HMDB0001170	-7.3
	HMDB0012458	-8.3		HMDB0001452	-7.3
	HMDB0000067	-8.2		HMDB0001830	-7.3
	HMDB0001903	-8.2		HMDB0001903	-7.3
	HMDB0000053	-8.1		HMDB0004977	-7.3
	HMDB0000908	-8.1		HMDB0004979	-7.3
	HMDB0001452	-8.1		HMDB0006278	-7.3
	HMDB0004659	-8.1		HMDB0007934	-7.3
	HMDB0010369	-8.1		HMDB0060824	-7.3
	HMDB0001830	-8		HMDB0000319	-7.2
	HMDB0001425	-7.9		HMDB0000145	-7.1
	HMDB0041917	-7.9		HMDB0001980	-7.1
	HMDB0060676	-7.9		HMDB0004659	-7.1
	HMDB0000319	-7.8		HMDB0001314	-7
	HMDB0000852	-7.8		HMDB0001547	-7
	HMDB0001547	-7.8		HMDB0060676	-7
	HMDB0006278	-7.8		HMDB0000058	-6.9
	HMDB0010404	-7.8		HMDB0000151	-6.9
	HMDB0000054	-7.7		HMDB0010404	-6.9
	HMDB0001980	-7.7		HMDB0000054	-6.8
	HMDB0002869	-7.7		HMDB0001425	-6.8
	HMDB0000037	-7.6		HMDB0003424	-6.8
	HMDB0000153	-7.6		HMDB0000908	-6.7
	HMDB0000706	-7.6		HMDB0041867	-6.7
	HMDB0006335	-7.6		HMDB0004246	-6.6
	HMDB0000145	-7.5		HMDB0041818	-6.6
	HMDB0000151	-7.5		HMDB0000706	-6.5
	HMDB0001375	-7.5		HMDB0029898	-6.5
	HMDB0041867	-7.5		HMDB0000195	-6.4

	HMDB0000305	-7.4		HMDB0014967	-6.4
	HMDB0000918	-7.4		HMDB0000248	-6.3
	HMDB0000265	-7.3		HMDB0000265	-6.3
	HMDB0001893	-7.3		HMDB0001220	-6.3
	HMDB0010370	-7.3		HMDB0015372	-6.3
	HMDB0000430	-7.2		HMDB0000095	-6.2
	HMDB0014967	-7.1		HMDB0000852	-6.2
	HMDB0060538	-7.1		HMDB0006335	-6.2
	HMDB0001314	-7		HMDB0060538	-6.2
	HMDB0006725	-7		HMDB0000133	-6.1
	HMDB0009331	-7		HMDB0000258	-6.1
	HMDB0013302	-7		HMDB0001438	-6.1
	HMDB0041818	-7		HMDB0002869	-6.1
	HMDB0000058	-6.9		HMDB0003337	-6.1
	HMDB0001220	-6.8		HMDB0001893	-6
	HMDB0010368	-6.8		HMDB0008714	-6
	HMDB0015532	-6.8		HMDB0000045	-5.9
	HMDB0015372	-6.8		HMDB0000299	-5.9
	HMDB0014488	-6.7		HMDB0000939	-5.9
	HMDB0001238	-6.6		HMDB0002028	-5.9
	HMDB0005453	-6.6		HMDB0003333	-5.9
	HMDB0061040	-6.6		HMDB0000430	-5.8
	HMDB0000248	-6.5		HMDB0002886	-5.8
	HMDB0000763	-6.5		HMDB0014703	-5.8
	HMDB0000929	-6.5		HMDB0006725	-5.7
	HMDB0008714	-6.5		HMDB0013302	-5.7
	HMDB0013609	-6.5		HMDB0010369	-5.6
	HMDB0000939	-6.4		HMDB0012110	-5.6
	HMDB0001438	-6.4		HMDB0000296	-5.5
	HMDB0006461	-6.4		HMDB0000767	-5.5
	HMDB0029898	-6.4		HMDB0013609	-5.5
	HMDB0000197	-6.3		HMDB0000378	-5.4
	HMDB0002028	-6.3		HMDB0000561	-5.4
	HMDB0000299	-6.2		HMDB0000929	-5.4
	HMDB0001285	-6.2		HMDB0001285	-5.4
	HMDB0009467	-6.2		HMDB0006736	-5.4
	HMDB0012110	-6.2		HMDB0010370	-5.4
	HMDB0014703	-6.2		HMDB0060994	-5.4
	HMDB0060947	-6.2		HMDB0000305	-5.3
	HMDB0000840	-6.1		HMDB0000840	-5.3
	HMDB0003337	-6.1		HMDB0000885	-5.3
	HMDB0007578	-6.1		HMDB0001238	-5.3
	HMDB0013339	-6.1		HMDB0001347	-5.3

	HMDB0000195	-6		HMDB0001434	-5.3
	HMDB0000714	-6		HMDB0003072	-5.3
	HMDB0003252	-6		HMDB0004148	-5.3
	HMDB0005464	-6		HMDB0014488	-5.3
	HMDB0005474	-6		HMDB0029865	-5.3
	HMDB0009093	-6		HMDB0000068	-5.2
	HMDB0029865	-6		HMDB0000639	-5.2
	HMDB0000095	-5.9		HMDB0000640	-5.2
	HMDB0000159	-5.9		HMDB0000763	-5.2
	HMDB0002043	-5.9		HMDB0000918	-5.2
	HMDB0004148	-5.9		HMDB0012109	-5.2
	HMDB0000122	-5.8		HMDB0013339	-5.2
	HMDB0000181	-5.8		HMDB0000125	-5.1
	HMDB0000258	-5.8		HMDB0000181	-5.1
	HMDB0000296	-5.8		HMDB0000318	-5.1
	HMDB0000684	-5.8		HMDB0000472	-5.1
	HMDB0000944	-5.8		HMDB0000684	-5.1
	HMDB0001336	-5.8		HMDB0000714	-5.1
	HMDB0001347	-5.8		HMDB0000824	-5.1
	HMDB0003070	-5.8		HMDB0001336	-5.1
	HMDB0004095	-5.8		HMDB0001490	-5.1
	HMDB0005066	-5.8		HMDB0006461	-5.1
	HMDB0005784	-5.8		HMDB0010368	-5.1
	HMDB0013338	-5.8		HMDB061695	-5.1
	HMDB0000045	-5.7		HMDB0000122	-5
	HMDB0000068	-5.7		HMDB0000197	-5
	HMDB0000209	-5.7		HMDB0000216	-5
	HMDB0001123	-5.7		HMDB0000289	-5
	HMDB0001999	-5.7		HMDB0000736	-5
	HMDB0005393	-5.7		HMDB0001847	-5
	HMDB0006275	-5.7		HMDB0002013	-5
	HMDB0006709	-5.7		HMDB0002030	-5
	HMDB0000259	-5.6		HMDB0003070	-5
	HMDB0000318	-5.6		HMDB0006351	-5
	HMDB0000640	-5.6		HMDB0013338	-5
	HMDB0001434	-5.6		HMDB0013856	-5
	HMDB0002030	-5.6		HMDB0000292	-4.9
	HMDB0003072	-5.6		HMDB0000660	-4.9
	HMDB0003080	-5.6		HMDB0001123	-4.9
	HMDB0004685	-5.6		HMDB0002012	-4.9
	HMDB0008957	-5.6		HMDB0004685	-4.9
	HMDB0012109	-5.6		HMDB0006275	-4.9
	HMDB0000125	-5.5		HMDB0009467	-4.9

	HMDB0000378	-5.5		HMDB0000020	-4.8
	HMDB0000660	-5.5		HMDB0000044	-4.8
	HMDB0000824	-5.5		HMDB0000159	-4.8
	HMDB0001490	-5.5		HMDB0000291	-4.8
	HMDB0006351	-5.5		HMDB0006709	-4.8
	HMDB0010383	-5.5		HMDB0009093	-4.8
	HMDB0013856	-5.5		HMDB0011635	-4.8
	HMDB0062769	-5.5		HMDB0041870	-4.8
	HMDB0000020	-5.4		HMDB0000118	-4.7
	HMDB0000118	-5.4		HMDB0000132	-4.7
	HMDB0000472	-5.4		HMDB0003252	-4.7
	HMDB0000767	-5.4		HMDB0003933	-4.7
	HMDB0000848	-5.4		HMDB0004369	-4.7
	HMDB0001043	-5.4		HMDB0010383	-4.7
	HMDB0002012	-5.4		HMDB0062555	-4.7
	HMDB0002183	-5.4		HMDB0036062	-4.7
	HMDB0003333	-5.4		HMDB0000209	-4.6
	HMDB0005454	-5.4		HMDB0000259	-4.6
	HMDB0061864	-5.4		HMDB0003414	-4.6
	HMDB0000073	-5.3		HMDB0004095	-4.6
	HMDB0000132	-5.3		HMDB0005065	-4.6
	HMDB0000222	-5.3		HMDB0005784	-4.6
	HMDB0002013	-5.3		HMDB0009331	-4.6
	HMDB0002712	-5.3		HMDB0000098	-4.5
	HMDB0004667	-5.3		HMDB0001403	-4.5
	HMDB0000133	-5.2		HMDB0002043	-4.5
	HMDB0000216	-5.2		HMDB0003080	-4.5
	HMDB0000736	-5.2		HMDB0004812	-4.5
	HMDB0001388	-5.2		HMDB0008957	-4.5
	HMDB0003208	-5.2		HMDB0000158	-4.4
	HMDB0004978	-5.2		HMDB0000679	-4.4
	HMDB0041870	-5.2		HMDB0002712	-4.4
	HMDB0000292	-5.1		HMDB0003208	-4.4
	HMDB0000529	-5.1		HMDB0061040	-4.4
	HMDB0001085	-5.1		HMDB0000072	-4.3
	HMDB0062558	-5.1		HMDB0000073	-4.3
	HMDB0000044	-5		HMDB0000157	-4.3
	HMDB0000207	-5		HMDB0000207	-4.3
	HMDB0001403	-5		HMDB0000283	-4.3
	HMDB0001847	-5		HMDB0000568	-4.3
	HMDB0003933	-5		HMDB0000807	-4.3
	HMDB0005065	-5		HMDB0000848	-4.3
	HMDB0007008	-5		HMDB0000904	-4.3

	HMDB0007158	-5		HMDB0002183	-4.3
	HMDB0011635	-5		HMDB0005066	-4.3
	HMDB0000306	-4.9		HMDB0005454	-4.3
	HMDB0002068	-4.9		HMDB0000208	-4.2
	HMDB0002259	-4.9		HMDB0000867	-4.2
	HMDB0004369	-4.9		HMDB0000943	-4.2
	HMDB0006710	-4.9		HMDB0002917	-4.2
	HMDB0000157	-4.8		HMDB0005457	-4.2
	HMDB0000283	-4.8		HMDB0005474	-4.2
	HMDB0000289	-4.8		HMDB0006710	-4.2
	HMDB0000291	-4.8		HMDB0062558	-4.2
	HMDB0002231	-4.8		HMDB0056381	-4.2
	HMDB0003418	-4.8		HMDB0000222	-4.1
	HMDB0000158	-4.7		HMDB0000510	-4.1
	HMDB0000162	-4.7		HMDB0000695	-4.1
	HMDB0000573	-4.7		HMDB0000958	-4.1
	HMDB0000885	-4.7		HMDB0001085	-4.1
	HMDB0003231	-4.7		HMDB0003231	-4.1
	HMDB0005457	-4.7		HMDB0007008	-4.1
	HMDB0000673	-4.6		HMDB0007098	-4.1
	HMDB0013622	-4.6		HMDB0061864	-4.1
	HMDB0029581	-4.6		HMDB0000162	-4
	HMDB0060994	-4.6		HMDB0000172	-4
	HMDB0000208	-4.5		HMDB0000247	-4
	HMDB0000679	-4.5		HMDB0000306	-4
	HMDB0000695	-4.5		HMDB0000517	-4
	HMDB0000826	-4.5		HMDB0000744	-4
	HMDB0033923	-4.5		HMDB0000784	-4
	HMDB0000172	-4.4		HMDB0001539	-4
	HMDB0000562	-4.4		HMDB0002005	-4
	HMDB0000639	-4.4		HMDB0004667	-4
	HMDB0000847	-4.4		HMDB0005453	-4
	HMDB0001863	-4.4		HMDB0031067	-4
	HMDB0002886	-4.4		HMDB0031125	-4
	HMDB0004812	-4.4		HMDB0033923	-4
	HMDB0035159	-4.4		HMDB0062556	-4
	HMDB0040598	-4.4		HMDB0000078	-3.9
	HMDB0062436	-4.4		HMDB0000529	-3.9
	HMDB0000098	-4.3		HMDB0000562	-3.9
	HMDB0007098	-4.3		HMDB0000883	-3.9
	HMDB0062555	-4.3		HMDB0003229	-3.9
	HMDB0000177	-4.2		HMDB0003334	-3.9
	HMDB0000182	-4.2		HMDB0005393	-3.9

	HMDB0000807	-4.2		HMDB0005464	-3.9
	HMDB0000958	-4.2		HMDB0006483	-3.9
	HMDB0010378	-4.2		HMDB0007158	-3.9
	HMDB0000134	-4.1		HMDB0007368	-3.9
	HMDB0000254	-4.1		HMDB0062769	-3.9
	HMDB0000744	-4.1		HMDB0000167	-3.8
	HMDB0000904	-4.1		HMDB0000575	-3.8
	HMDB0002005	-4.1		HMDB0000687	-3.8
	HMDB0002368	-4.1		HMDB0000806	-3.8
	HMDB0003229	-4.1		HMDB0000847	-3.8
	HMDB0003339	-4.1		HMDB0001565	-3.8
	HMDB0006483	-4.1		HMDB0001999	-3.8
	HMDB0031125	-4.1		HMDB0002000	-3.8
	HMDB0000060	-4		HMDB0002231	-3.8
	HMDB0000072	-4		HMDB0002259	-3.8
	HMDB0000078	-4		HMDB0003339	-3.8
	HMDB0000112	-4		HMDB0004136	-3.8
	HMDB0000192	-4		HMDB0004978	-3.8
	HMDB0000247	-4		HMDB0007578	-3.8
	HMDB0000357	-4		HMDB0062436	-3.8
	HMDB0000510	-4		HMDB0000134	-3.7
	HMDB0000784	-4		HMDB0000168	-3.7
	HMDB0000827	-4		HMDB0000177	-3.7
	HMDB0000883	-4		HMDB0000182	-3.7
	HMDB0007368	-4		HMDB0000220	-3.7
	HMDB0000039	-3.9		HMDB0000573	-3.7
	HMDB0000517	-3.9		HMDB0000827	-3.7
	HMDB0000696	-3.9		HMDB0000944	-3.7
	HMDB0000806	-3.9		HMDB0001388	-3.7
	HMDB0000943	-3.9		HMDB0029581	-3.7
	HMDB0001539	-3.9		HMDB0035215	-3.7
	HMDB0003424	-3.9		HMDB0000254	-3.6
	HMDB0031067	-3.9		HMDB0000826	-3.6
	HMDB0000161	-3.8		HMDB0001863	-3.6
	HMDB0000190	-3.8		HMDB0002068	-3.6
	HMDB0000220	-3.8		HMDB0013622	-3.6
	HMDB0000243	-3.8		HMDB0015576	-3.6
	HMDB0000568	-3.8		HMDB0040598	-3.6
	HMDB0000687	-3.8		HMDB0000060	-3.5
	HMDB0000870	-3.8		HMDB0000187	-3.5
	HMDB0002917	-3.8		HMDB0000192	-3.5
	HMDB0003334	-3.8		HMDB0000357	-3.5
	HMDB0000043	-3.7		HMDB0000696	-3.5

	HMDB0000187	-3.7		HMDB0003418	-3.5
	HMDB0000214	-3.7		HMDB0010378	-3.5
	HMDB0001310	-3.7		HMDB0000043	-3.4
	HMDB0001565	-3.7		HMDB0000214	-3.4
	HMDB0002000	-3.7		HMDB0000870	-3.4
	HMDB0015576	-3.7		HMDB0002994	-3.4
	HMDB0062556	-3.7		HMDB0035159	-3.4
	HMDB0000056	-3.6		HMDB0000112	-3.3
	HMDB0000131	-3.6		HMDB0001043	-3.3
	HMDB0000167	-3.6		HMDB0002368	-3.3
	HMDB0000168	-3.6		HMDB0000131	-3.2
	HMDB0000251	-3.5		HMDB0000190	-3.2
	HMDB0000867	-3.5		HMDB0000243	-3.2
	HMDB0000575	-3.4		HMDB0000251	-3.2
	HMDB0001881	-3.4		HMDB0002329	-3.2
	HMDB0002329	-3.4		HMDB0000039	-3.1
	HMDB0002994	-3.4		HMDB0000056	-3.1
	HMDB0004136	-3.4		HMDB0000097	-3.1
	HMDB0000115	-3.2		HMDB0000161	-3.1
	HMDB0000097	-3.1		HMDB0000673	-3.1
	HMDB0006112	-3.1		HMDB0001310	-3.1
	HMDB0000257	-3		HMDB0000257	-3
	HMDB0000925	-3		HMDB0000115	-2.9
	HMDB0001429	-3		HMDB0001429	-2.9
	HMDB0001448	-3		HMDB0001448	-2.9
	HMDB0000595	-2.8		HMDB0001881	-2.9
	HMDB0002878	-2.8		HMDB0002786	-2.8
	HMDB0000294	-2.6		HMDB0002878	-2.8
	HMDB0000149	-2.4		HMDB0006112	-2.8
	HMDB0002786	-2.2		HMDB0000595	-2.7
	HMDB0000464	-1.9		HMDB0000925	-2.7
	HMDB0000547	-1.9		HMDB0000294	-2.3
	HMDB0000586	-1.9		HMDB0000149	-2.2
	HMDB0015531	-1.9		HMDB0003125	-2
	HMDB0001875	-1.6		HMDB0001875	-1.6
	HMDB0003338	-1.6		HMDB0003338	-1.6
	HMDB0003378	-1.6		HMDB0003378	-1.6
	HMDB0003125	-1.5		HMDB0002500	-1.4
	HMDB0002500	-1.3		HMDB0000464	-1.2

Supplementary table 3: Antigenicity of novel membrane proteins (Vaccine targets) and similarity analysis with human microbiome

Protein ID	Vaxijen Score	Similarity	Prediction
Q87P28	0.4458	68	ANTIGEN
Q87HY1	0.3452	42	NON-ANTIGEN
Q87TD7	0.5575	56	ANTIGEN
Q87GB4	0.4450	52	ANTIGEN
Q87P22	0.5721	49	ANTIGEN
Q87JA2	0.7064	72	ANTIGEN
Q87Q13	0.5984	50	ANTIGEN
Q87R85	0.4509	62	ANTIGEN
Q79YZ4	0.3205	68	NON-ANTIGEN
Q87P56	0.4949	76	ANTIGEN
Q79YT9	0.5180	74	ANTIGEN
Q87FY4	0.6195	45	ANTIGEN
Q87P44	0.4034	67	ANTIGEN
Q79YY3	0.6429	60	ANTIGEN
Q87FM8	0.4523	51	ANTIGEN
Q87J60	0.6522	60	ANTIGEN
Q87LX8	0.4736	63	ANTIGEN
Q87LX7	0.5144	59	ANTIGEN
Q87HJ8	0.6461	45	ANTIGEN
Q87GB2	0.5797	48	ANTIGEN
Q87JH9	0.5311	41	ANTIGEN
Q87GY3	0.5303	45	ANTIGEN
Q87Q18	0.3866	42	NON-ANTIGEN
Q87FX8	0.7299	71	ANTIGEN
Q87IQ2	0.3443	47	NON-ANTIGEN

Supplementary table 4: Antigenicity and similiarity analysis of novel outer membrane proteins with human microbiome (%)

Accession No.	Vaxijen Score	Similiarity analysis with human microbiome (%)
Q87P28	0.4458	<68
Q87HY1	0.3452	<42
Q87TD7	0.5575	<56
Q87GB4	0.4450	<52
Q87P22	0.5721	<49
Q87JA2	0.7064	<72
Q87Q13	0.5984	<50
Q87R85	0.4509	<62
Q79YZ4	0.3205	<68
Q87P56	0.4949	<76
Q79YT9	0.5180	<74
Q87FY4	0.6195	<45
Q87P44	0.4034	<67
Q79YY3	0.6429	<60
Q87FM8	0.4523	<51
Q87J60	0.6522	<60
Q87LX8	0.4736	<63
Q87LX7	0.5144	<59
Q87HJ8	0.6461	<45
Q87GB2	0.5797	<48
Q87JH9	0.5311	<41
Q87GY3	0.5303	<45
Q87Q18	0.3866	<42
Q87FX8	0.7299	<71
Q87IQ2	0.3443	<47

Supplementary table 5: Allergenicity pattern and toxicity analysis of top epitopes for Sensor histidine protein kinase and Flagellar hook-associated protein

Protein	Epitope	Vaxijen	Allertop	Allergen FP	Allermatch	Allergen Online	Toxin Pred
Sensor histidine protein kinase	DPELAILLFPFALRL	2.2869	Allergen	Non-Allergen	Allergen	Non-Allergen	Non-Toxin
	LMLVPMCYLLWNYLF	2.1611	Allergen	Non-Allergen	Non-Allergen	Non-Allergen	Non-Toxin
	ILLFPFALRLGIALH	2.1484	Non-Allergen	Non-Allergen	Non-Allergen	Non-Allergen	Non-Toxin
	LAILLFPFALRLGIA	2.1118	Non-Allergen	Non-Allergen	Allergen	Non-Allergen	Non-Toxin
	PELAILLFPFALRLG	2.0796	Allergen	Non-Allergen	Allergen	Non-Allergen	Non-Toxin
	VNDPELAILLFPFAL	2.0618	Allergen	Non-Allergen	Allergen	Non-Allergen	Non-Toxin
	ELAILLFPFALRLGI	2.0569	Non-Allergen	Non-Allergen	Allergen	Non-Allergen	Non-Toxin
	ACAWFCLWVIAYYFV	1.9635	Allergen	Non-Allergen	Non-Allergen	Non-Allergen	Toxin
	AILLFPFALRLGIAL	1.9451	Non-Allergen	Non-Allergen	Non-Allergen	Non-Allergen	Non-Toxin
	WFCLWVIAYYFVNDP	1.9417	Allergen	Non-Allergen	Non-Allergen	Non-Allergen	Non-Toxin
	NDPELAILLFPFALR	1.8981	Allergen	Non-Allergen	Allergen	Non-Allergen	Non-Toxin
	MLVPMCYLLWNYLFQ	1.844	Allergen	Non-Allergen	Non-Allergen	Non-Allergen	Non-Toxin
	LLFPFALRLGIALHT	1.8268	Non-Allergen	Allergen	Non-Allergen	Non-Allergen	Non-Toxin
	CAWFCLWVIAYYFVN	1.8066	Allergen	Allergen	Non-Allergen	Non-Allergen	Non-Toxin
	VMACAWFCLWVIAYY	1.7285	Allergen	Allergen	Non-Allergen	Non-Allergen	Toxin
	AILLFPFAL	2.993	Non-Allergen	Allergen	Non-Allergen	Non-Allergen	Non-Toxin
	ILLFPFALR	2.9721	Non-Allergen	Allergen	Non-Allergen	Non-Allergen	Non-Toxin
	FCLWVIAYYF	2.8883	Allergen	Non-Allergen	Non-Allergen	Non-Allergen	Non-Toxin
	CYLLWNYLF	2.8253	Allergen	Allergen	Non-Allergen	Non-Allergen	Non-Toxin
	ELAILLFPF	2.7265	Non-Allergen	Allergen	Allergen	Non-Allergen	Non-Toxin
	LLFPFALRL	2.7071	Allergen	Non-Allergen	Non-Allergen	Non-Allergen	Non-Toxin

	LAILLFPFA	2.6785	Non-Allergen	Allergen	Allergen	Non-Allergen	Non-Toxin
	WFCLWVIAY	2.5591	Allergen	Allergen	Non-Allergen	Non-Allergen	Non-Toxin
	LWVIAYYFV	2.4774	Non-Allergen	Allergen	Non-Allergen	Non-Allergen	Non-Toxin
	HDDGVGFKV	2.363	Non-Allergen	Non-Allergen	Non-Allergen	Non-Allergen	Non-Toxin
	YLLWNYLFQ	2.3399	Allergen	Allergen	Non-Allergen	Non-Allergen	Non-Toxin
	DDGVGFKVQ	2.325	Allergen	Non-Allergen	Non-Allergen	Non-Allergen	Non-Toxin
	DGVGFKVQD	2.1287	Allergen	Non-Allergen	Non-Allergen	Non-Allergen	Non-Toxin
Flagellar hook-associated protein	DSIESSFNAQDEEGH	1.304	Non-Allergen	Non-Allergen	Non-Allergen	Non-Allergen	Non-Toxin
	PNFQAEVDASLNAID	1.146	Allergen	Non-Allergen	Non-Allergen	Non-Allergen	Non-Toxin
	SGAYVVEGNSDVRVV	1.06	Allergen	Non-Allergen	Non-Allergen	Non-Allergen	Non-Toxin
	AEFEKPSPNFQAEVD	1.056	Allergen	Non-Allergen	Non-Allergen	Non-Allergen	Non-Toxin
	GGRHNNLDLMDGAHS	0.964	Non-Allergen	Non-Allergen	Non-Allergen	Non-Allergen	Non-Toxin
	GAYVVEGNSDVRVVT	0.92	Allergen	Allergen	Non-Allergen	Non-Allergen	Non-Toxin
	KLSDDPMASIKLLNL	0.887	Non-Allergen	Allergen	Non-Allergen	Non-Allergen	Non-Toxin
	NFQAEVDASLNAIDD	0.8431	Allergen	Allergen	Non-Allergen	Non-Allergen	Non-Toxin
	EVDASLNAIDDTMAN	0.832	Allergen	Non-Allergen	Non-Allergen	Non-Allergen	Non-Toxin
	MMLQSLQSNSAGLGK	0.819	Non-Allergen	Non-Allergen	Non-Allergen	Non-Allergen	Non-Toxin
	IGGRHNNLDLMDGAH	0.801	Non-Allergen	Non-Allergen	Non-Allergen	Non-Allergen	Non-Toxin
	KVSGDLSALDYGEAS	0.751	Non-Allergen	Non-Allergen	Non-Allergen	Non-Allergen	Non-Toxin
	LNKSSGAYVVEGNSD	0.701	Non-Allergen	Non-Allergen	Non-Allergen	Non-Allergen	Non-Toxin
	GGGKNVLNQIDALIA	0.639	Allergen	Non-Allergen	Non-Allergen	Non-Allergen	Non-Toxin
	VDASLNAIDDTMANV	0.625	Non-Allergen	Non-Allergen	Non-Allergen	Non-Allergen	Non-Toxin
	LDIGGGKNV	1.9185	Non-Allergen	Allergen	Non-Allergen	Non-Allergen	Non-Toxin

	GANGSLTDQ	1.8499	Allergen	Allergen	Non-Allergen	Non-Allergen	Non-Toxin
	FNAQDEEGH	1.8425	Non-Allergen	Allergen	Non-Allergen	Non-Allergen	Non-Toxin
	SFNAQDEEG	1.8224	Allergen	Allergen	Non-Allergen	Non-Allergen	Non-Toxin
	SPNFQAEVD	1.7972	Allergen	Allergen	Non-Allergen	Non-Allergen	Non-Toxin
	GGRHNNLDL	1.7855	Allergen	Non-Allergen	Non-Allergen	Non-Allergen	Non-Toxin
	PNFQAEVDA	1.7403	Allergen	Non-Allergen	Non-Allergen	Non-Allergen	Non-Toxin
	KPSPNFQAE	1.7093	Allergen	Non-Allergen	Non-Allergen	Non-Allergen	Non-Toxin
	DIGGGKNVL	1.662	Non-Allergen	Allergen	Non-Allergen	Non-Allergen	Non-Toxin
	NFQAEVDAS	1.5455	Allergen	Allergen	Non-Allergen	Non-Allergen	Non-Toxin
	SSFNAQDEEG	1.5143	Allergen	Allergen	Non-Allergen	Non-Allergen	Non-Toxin
	KPSPNFQAEV	1.4978	Non-Allergen	Non-Allergen	Non-Allergen	Non-Allergen	Non-Toxin
	LQSNSAGLG	1.4717	Non-Allergen	Allergen	Non-Allergen	Non-Allergen	Non-Toxin

Supplementary Table 6: Allergenicity assessment of the predicted B-cell epitopes generated from histidine protein kinase and flagellar hook-associated protein

Protein	Start	End	Peptide	Length	Allergenicity	Algorithm
Histidine protein kinase UhpB	6	20	VTTICGLFVMACAWF	15	Non Allergen	Linear epitope
	100	106	YYYGDQN	7	Non Allergen	Beta turn
	272	283	VQKQKDLNHKLR	12	Non Allergen	Surface accessibility
	353	359	YDTTKRL	7	Non Allergen	Flexibility
	207	222	FAPFCMAIPIIVLALR	16	Non Allergen	Antigeneicity
	271	277	AVQKQKD	7	Non Allergen	hydrophilicity
Flagellar hook-associated protein	201	211	FEKPSPNFQAE	11	Non Allergen	Linear epitope
	147	153	NKSSGAY	7	Non Allergen	Beta turn
	29	43	QMSTRERLTKLSDDP	15	Non Allergen	Surface accessibility
	73	79	LSSQETH	6	Non Allergen	Flexibility
	161	167	VRVVTVA	7	Non Allergen	Antigeneicity
	138	144	GTKTDTA	7	Non Allergen	Hydrophilicity

Supplementary Table 7: Allergenicity, antigenicity and solubility prediction of the constructed vaccines

Constructs	Composition	Complete Sequence of Vaccine Constructs	Antigenicity (Threshold 0.4)	Allergenicity	Solubility (Threshold 0.45)
V1	Predicted CTL, HTL & BCL epitopes with β defensin adjuvant & PADRE sequence	**EAAAK**GIINTLQKYYCRVRGGRCAVLSCLPKEEQIGKCSTRG RKCCRRKK**EAAAK**AKFVAAWTLKAAA**GGGS**AILLFPFALR **GGGS**HDDGVGFKV**GGGS**FNAQDEEGH**GGGS**GGRHNNLDL **GGGS**KPSPNFQAEV**GPGPG**AILLFPFALRLGIALHT**GPGPG**D SIESSFNAQDEEGH**GPGPG**IGGRHNNLDLMDGAH**GPGPG**KL SDDPMASIKLLNL**KK**VTTICGLFVMACAWF**KK**YYYGDQN**K K**AVQKQKDLNHKLR**KK**YDTTKRL**KK**FAPFCMAIPIIVLALR **KK**FEKPSPNFQAE**KK**NKSSGAY**KK**QMSTRERLTKLSDDP**KK** LSSQETH**KK**VRVVTVA**KK**GTKTDTA**KK**AKFVAAWTLKAAA **GGGS**	1.18	Non Allergen	0.661
V2	Predicted CTL, HTL & BCL epitopes with L7/L12 ribosomal protein adjuvant & PADRE sequence	**EAAAK**MAKLSTDELLDAFKEMTLLELSDFVKKFEETFEVTAA APVAVAAAGAAPAGAAVEAAEEQSEFDVILEAAGDKKIGVIK VVREIVSGLGLKEAKDLVDGAPKPLLEKVAKEAADEAKAKL EAAGATVTVK**EAAAK**AKFVAAWTLKAAA**GGGS**AILLFPFAL R**GGGS**HDDGVGFKV**GGGS**FNAQDEEGH**GGGS**GGRHNNLD L**GGGS**KPSPNFQAEV**GPGPG**AILLFPFALRLGIALHT**GPGPG** DSIESSFNAQDEEGH**GPGPG**IGGRHNNLDLMDGAH**GPGPG**K LSDDPMASIKLLNL**KK**VTTICGLFVMACAWF**KK**YYYGDQN **KK**AVQKQKDLNHKLR**KK**YDTTKRL**KK**FAPFCMAIPIIVLAL R**KK**FEKPSPNFQAE**KK**NKSSGAY**KK**QMSTRERLTKLSDDP**K K**LSSQETH**KK**VRVVTVA**KK**GTKTDTA**KK**AKFVAAWTLKA AA**GGGS**	1.00	Non Allergen	0.603
V3	Predicted CTL, HTL & BCL epitopes with HABA adjuvant & PADRE sequence	**EAAAK**MAENPNIDDLPAPLLAALGAADLALATVNDLIANLR ERAEETRAETRTRVEERRARLTKFQEDLPEQFIELRDKFTTEE LRKAAEGYLEAATNRYNELVERGEAALQRLRSQTAFEDASA RAEGYVDQAVELTQEALGTVASQTRAVGERAAKLVGIEL**EA AAK**AKFVAAWTLKAAA**GGGS**AILLFPFALR**GGGS**HDDGVG FKV**GGGS**FNAQDEEGH**GGGS**GGRHNNLDL**GGGS**KPSPNFQ AEV**GPGPG**AILLFPFALRLGIALHT**GPGPG**DSIESSFNAQDEE GH**GPGPG**IGGRHNNLDLMDGAH**GPGPG**KLSDDPMASIKLL NL**KK**VTTICGLFVMACAWF**KK**YYYGDQN**KK**AVQKQKDLN HKLR**KK**YDTTKRL**KK**FAPFCMAIPIIVLALR**KK**FEKPSPNFQA E**KK**NKSSGAY**KK**QMSTRERLTKLSDDP**KK**LSSQETH**KK**VRV VTVA**KK**GTKTDTA**KK**AKFVAAWTLKAAA**GGGS**	1.03	Non Allergen	0.625

Supplementary Table 8: Docking score of vaccine construct V1, V2 and V3 with different HLA alleles including HLADRB1*03:01 (1A6A), HLA-DRB5*01:01 (1H15), HLA-DRB1*04:01 (2SEB), HLA-DRB3*01:01 (2Q6W), HLA-DRB1*01:01 (2FSE) and HLA-DRB3*02:02 (3C5J).

Vaccine Construct	HLA alleles PDB ID's	Global Energy	Hydrogen Bond Energy	ACE	Score	Area
V1	1A6A	-5.77	0.00	-2.93	15800	2614.80
	1H15	-32.57	-1.48	-3.79	16644	2074.50
	2SEB	-26.95	-2.39	2.40	17546	2082.60
	2Q6W	-16.57	-1.50	3.50	15770	2538.40
	2FSE	-19.27	-5.69	8.65	16988	2105.90
	3C5J	11.34	-1.87	2.10	16094	2066.20
V2	1A6A	-22.98	-2.20	-3.85	15152	2094.40
	1H15	-18.21	-2.99	11.23	16964	2574.80
	2Q6W	-1.13	0.00	4.11	18528	3097.60
	2SEB	4.86	0.00	4.62	17698	2379.80
	2FSE	-43.58	-5.18	2.59	16638	2311.70
	3C5J	-4.64	-1.04	1.32	18134	2927.80
V3	1A6A	-0.58	-1.24	4.86	17262	2533.10
	1H15	11.12	-1.51	8.43	18698	2572.80
	2SEB	17.22	0.00	3.91	21978	3151.80
	2Q6W	-16.11	-4.54	13.23	16068	2515.50
	2FSE	-11.82	-6.92	18.45	16308	2064.50
	3C5J	-5.73	-0.98	6.61	17746	2873.70